




Review

# Bio-Templating: An Emerging Synthetic Technique for Catalysts. A Review

M. Carmen Herrera-Beurnio, Jesús Hidalgo-Carrillo <sup>\*</sup>, Francisco J. López-Tenllado <sup>\*</sup>, Juan Martín-Gómez, Rafael C. Estévez , Francisco J. Urbano  and Alberto Marinas 

Departamento de Química Orgánica, Instituto Universitario de Investigación en Química Fina y Nanoquímica (IUNAN), Universidad de Córdoba, Campus de Rabanales, Edificio Marie Curie, E-14071 Córdoba, Spain; b52hebem@uco.es (M.C.H.-B.); juanmartingomez@outlook.es (J.M.-G.); q72estor@uco.es (R.C.E.); fj.urbano@uco.es (F.J.U.); alberto.marinas@uco.es (A.M.)

<sup>\*</sup> Correspondence: q12hica@uco.es (J.H.-C.); b42lotef@uco.es (F.J.L.-T.)

**Abstract:** In the last few years, researchers have focused their attention on the synthesis of new catalyst structures based on or inspired by nature. Biotemplating involves the transfer of biological structures to inorganic materials through artificial mineralization processes. This approach offers the main advantage of allowing morphological control of the product, as a template with the desired morphology can be pre-determined, as long as it is found in nature. This way, natural evolution through millions of years can provide us with new synthetic pathways to develop some novel functional materials with advantageous properties, such as sophistication, miniaturization, hybridization, hierarchical organization, resistance, and adaptability to the required need. The field of application of these materials is very wide, covering nanomedicine, energy capture and storage, sensors, biocompatible materials, adsorbents, and catalysis. In the latter case, bio-inspired materials can be applied as catalysts requiring different types of active sites (i.e., redox, acidic, basic sites, or a combination of them) to a wide range of processes, including conventional thermal catalysis, photocatalysis, or electrocatalysis, among others. This review aims to cover current experimental studies in the field of biotemplating materials synthesis and their characterization, focusing on their application in heterogeneous catalysis.

**Keywords:** bio-templating; bio-templated; bio-inspired; catalyst



**Citation:** Herrera-Beurnio, M.C.; Hidalgo-Carrillo, J.; López-Tenllado, F.J.; Martín-Gómez, J.; Estévez, R.C.; Urbano, F.J.; Marinas, A. Bio-Templating: An Emerging Synthetic Technique for Catalysts. A Review. *Catalysts* **2021**, *11*, 1364. <https://doi.org/10.3390/catal11111364>

Academic Editor: Omid Akhavan

Received: 8 October 2021

Accepted: 11 November 2021

Published: 12 November 2021

**Publisher's Note:** MDPI stays neutral with regard to jurisdictional claims in published maps and institutional affiliations.



**Copyright:** © 2021 by the authors. Licensee MDPI, Basel, Switzerland. This article is an open access article distributed under the terms and conditions of the Creative Commons Attribution (CC BY) license (<https://creativecommons.org/licenses/by/4.0/>).

## 1. Introduction

Nature has been perfecting materials and biological systems through evolution over thousands of years, developing a rather complex hierarchy at all levels to adapt to the constant modifications of the environment. Those years of evolution provided natural materials with some useful features such as resistance, adaptability, and sophistication [1]. The optimization of the use of materials and energy in nature makes it extremely interesting to science, as it can learn from these biological materials and systems by taking advantage of their intricate structures or mechanisms of action through their replication to develop functional materials [2,3].

In the past two decades, the field of biotemplating has emerged as a new way of engineering those new inorganic functional materials inspired by nature [4]. The foundation of the biotemplating technique is based on the incorporation of the desired inorganic compounds on the natural template followed by mineralization processes that occur naturally, where organic compounds of the templates disappear through degradation [5]. This entails the transfer of biological structures into inorganic materials through natural mineralization (fossilization) or artificial processes, allowing for the development of extremely intricate structures that replicate the different scales of hierarchy of natural materials used as templates. The process through which the bioinspired composites are obtained is mainly divided into three phases, where after preparing the sample and depositing the inorganic

material on the organic template, the natural pattern is mainly removed through thermal treatments depending on the desired result of the new material or the actual template [6]. For example, Hashemizadeh et al. [1] designed some catalysts using *Camellia* tree leaves. For that, they first washed, cut, and dried the leaves (preparation phase), then they added  $\text{TiCl}_3$  as a precursor for the incorporation of the inorganic material (second phase), and lastly, they calcined the synthesized catalyst at 773 K to remove the organic template (third phase).

The main templates that are used to replicate the nanoscale, or that are said to be useful, are molecules such as native or modified proteins, DNA, microtubules, or cellulose [6,7]. Proteins have been used in many studies to fabricate materials such as nanotubes or nanospheres since they are naturally able to display catalytic and structural functions and are biocompatible and biodegradable. Protein crystals are of great interest as well, as their structures allow for the development of 3D crystalline composites with potential applications in different fields [8,9]. Self-assembly of biological molecules is one of the characteristics that scientists are most interested in. Self-assembled DNA is a very useful template as it can be used as a scaffold to design nanoparticles or nanowires and its nitrogen and oxygen rich structure improves the binding capacity to transition metal ions during the synthesis of inorganic materials through biotemplating [10,11]. Also, viral envelopes, bacterial cell surface layer proteins, microalgae, both eukaryotic and procaryotic cells, and biofilms are of great interest [12–15]. In particular, rod-like viruses such as the tobacco mosaic virus provide an attractive approach because their hollow structures offer a viable template to guide the synthesis of nanoparticles and control their sizes and constitution [16]. Another virus that has been used as a pattern for biotemplating approaches is the M13 phage, as its genetically engineered mutants present modifications on the surface that bind to nanoparticles or nanotubes, improving the functionality of the material [17]. Wood [18], cotton [19], aquatic plants [20], green leaves [1,21], or even animal products [22] have also been used as templates. Butterfly wings are of great interest as they present an intricate and complex microstructure and photonic resonances that control their structural color and make them very suitable for catalysis and electrochemical applications [23–25]. As the nanometer scale of natural templates has been replicated, the wide variety of prepared materials have many potential applications [5,26]. These applications (catalysis, sensors, cancer therapy, tissue engineering, energy capture and storage, adsorbents, etc.) were considered to categorize the publications included in this review; after a more conscious reading of the texts, all papers were classified into these categories depending on the application that authors gave to the designed materials. The use of biotemplated materials in these fields will be seen in more depth in the following sections. Although in the past the background of this technique, the templates, and the applications in which the products are used have been reviewed [27,28], our paper summarizes the current applications of the techniques, focusing on catalysis and challenges that may be encountered in the future.

The relevance of biotemplating can be observed in the gradual increase in the number of publications appearing in Scopus between 2000 and June 2021 (Figure 1a). To perform this review, a search was conducted in the Scopus database limiting the type of document to article and review. The search used the following keywords: “biotemplating” and “bio-templating”. After joining the results obtained from both keywords and excluding duplicates, 220 publications were included in this review.

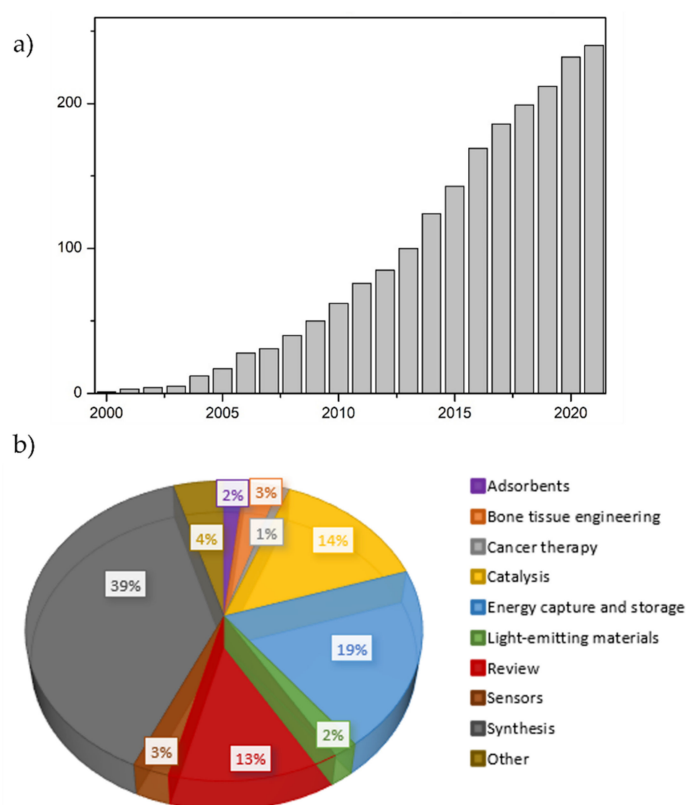


**Figure 1.** (a) Total accumulated number of publications appearing in the Scopus database from 2000 until June 2021 after removing duplicates found through “biotemplating” and “bio-templating” keyword data searching. (b) Scope of the different papers on biotemplating appearing in Scopus from 2000 to June 2021.

As has been mentioned before, bioinspired materials have many potential applications (Figure 1b). The first publications focusing on biotemplating only described the route through which the material was developed. However, they were not applied to any specific field. These papers were limited to the description of the synthetic approach and account for about 39% of those found in Scopus. Catalysis (14%) and energy capture and storage (19%) are the main applications of these bioinspired materials in the publications.

Among the reviews (accounting for 13% of the total), some of them focused on biotemplating, highlighting the importance of specific templates such as diatoms [29], polysaccharides [30–32], DNA [10], proteins [33], fluorescent modified amino acids [34], or butterfly wings [35], whereas Sotiropoulou et al. reviewed all biological templates that had been used up to 2008 [36]. Others focused on the use of this technique in the production of metal oxides [37,38], ceramics [39], inorganic materials [40], organic semiconductors [41], optical functional materials [42,43], and noble metal nanoparticles [44] via different methods and templates.

## 2. Applications

### 2.1. Adsorbents

In analytical chemistry, the control of sample preparation is essential to guarantee the isolation of an analyte at low concentration to improve its limit of detection. Although there are different sample preparation methods depending on the extraction phase, solid phase extraction (SPE) is the most used technique as it is a rapid and less arduous method [45,46]. In SPE, the analyte-containing solvent interacts with a sorbent material that has a high affinity for the analyte that needs to be isolated [47]. Due to the internal layered organization and porous structure of natural materials, biotemplating has been of great interest to develop adsorbents with improved adsorption capacity and to reduce the limitations of

current commercial adsorbents, including high cost, pH instability and a difficult synthesis process [46,48]. These adsorbents have been used for different purposes.

Reducing pollution of aqueous samples is essential as it is a serious threat for human health and the environment. Wang et al. [46] prepared an adsorbent using eggshell membranes (ESMs), a by-product of the food industry, as a template. As ESM was subjected to strong acidic conditions, the basic groups (e.g., amino groups,  $\text{NH}_2$ ) on ESMs were protonated to produce a positively charged surface. Subsequently, an anionic surfactant, linear alkylbenzene sulfonates, was added to the ESM and bound to its surface through electrostatic interaction resulting in the formation of hemimicelle/admicelle aggregates on the ESM that acted as adsorbents for polycyclic aromatic hydrocarbons (PAHs) from water samples. Also, the macroporous structure of eggshells has great permeability due to its protein fibers. The results of this experiment showed that using ESM as a template to manufacture an adsorbent for SPE had some advantages as it preconcentrates PAHs in the sample, and it is a low-cost and biocompatible material. Also, removing PAHs from water was the priority in another study where the authors prepared magnetically activated carbon nanocomposites from green tea leaves waste. The adsorbents showed high adsorption rates (86–98%) when they were applied to mineral water and could remove PAHs from tap water completely, which suggests that this templated-adsorbent might be useful for removing those pollutants from food wastewaters [49]. In another study [48], researchers developed a 3D porous-structure nanosheet of MgAl-layered double hydroxide anchored on carbon fibers using cotton as the template to remove organic dyes from water. Congo red was used as a model water pollutant to demonstrate the adsorption capacity of the material. The use of carbon fibers resulted in a significant increase in surface area ( $27.5 \text{ m}^2 \text{ g}^{-1}$  and  $90.3 \text{ m}^2 \text{ g}^{-1}$  for conventional MgAl-layered double hydroxide and the sample anchored on carbon fibers, respectively) due to the presence of mesopores of a smaller size than the ones of traditional Mg-Al layered double hydroxide (3.34 nm compared to 3.49 nm of Mg-Al layered double hydroxide). This resulted in the adsorption of Congo red being 60% higher on carbon fibers-modified solids with the adsorption/desorption capacity being maintained after four adsorption/desorption cycles.

In clinical biochemistry, Ghani [45] developed a porous titania film as an adsorbent for the isolation of analytes (e.g., nonsteroidal anti-inflammatory drugs) in urine by biotemplating with nanocrystalline cellulose derived from cotton fibers. The use of nanocrystalline cellulose as the template restricted the growth of titania crystals due to the narrow space between the crystals in the crystalline structure, thus resulting in a highly porous system (surface area of 165 and  $32 \text{ m}^2 \text{ g}^{-1}$  for templated and untreated titania, respectively). The authors did not perform a comparative study with other templates, though they pointed out shape persistence, higher temperature, and tuneable dimensions as some advantages of their approach compared to traditionally used “soft templates”. All in all, the limit of detection was found to be between the range of 0.2 and  $0.5 \mu\text{g L}^{-1}$  for all the nonsteroidal anti-inflammatory drugs that were tested in this article.

Water deficiency can have many impacts on health and the environment. Therefore, water harvesting by generating water from collected rain is essential in areas where fresh water is scarce. Suvindran et al. [50] assessed the wettability of *Tradescantia pallida*, an invasive species that can survive through drought and in arid places because it uses humidity from the environment. The authors determined that the leaves have an efficient dual way water harvesting system via the para-hydrophobic surface and the hydrophobic trichomes guiding the water along parallel channels. They subsequently developed a replica applying the conventional two-step biotemplating technique and using polypropylene pearl wool fibres to mimic the trichomes. It exhibited a similar hierarchical structure and wettability. Although more studies are needed to prove its efficiency, it was proposed that this material could be useful for a water harvesting system.

## 2.2. Cancer Therapy

Cancer is one of the main causes of death among humans in developed countries. Chemotherapy is a rather invasive treatment as it attacks both carcinogenic and normal cells. Therefore, research into targeted therapy is of prime importance to find treatments that are directed only towards tumor cells. The most promising techniques that are being studied are photothermal and photodynamic therapies, where applying local heat to cancerous cells and a chain of photochemical reactions derived from a photoactivated molecule, respectively, attacks cancer cells in a targeted way. Also, applying nanotechnology to therapies can have a major impact on the development of new treatments as nanomaterials can penetrate targeted tissue easily owing to their miniscule size. Furthermore, combining nanotechnology and photothermal therapy provides medicine with green technologies to help treat this disease. Although without the use of biotemplating, that combination is what Akhavan and Ghaderi [51] evaluated after preparing graphene oxide nanostructures with a high efficiency in reducing tumor size (100% tumor elimination after 48 h of injecting concentrations of  $10 \mu\text{g mL}^{-1}$  of the graphene material), due to graphene's capacity to absorb near infrared spectra and the nanoscale of the synthesized products, which provided the material with better penetration capability and retention in the tumor. Jiang et al. [52], using targeted graphene oxide nanostructures, combined photodynamic therapy and targeted drug delivery, as they developed some nanoplatfoms that absorbed the near infrared spectra and could release drugs, resulting in a more aggressive destruction of the tumor. Similar results were obtained by Lima-Sousa et al. [53], who functionalized reduced graphene oxide with hyaluronic acid to attack CD44, a glycoprotein that is in charge of tumor metastasis. They developed nanostructures that efficiently ablated cancer cells after being irradiated with a laser, obtaining a cancer cell viability of  $\sim 10\%$ . Green tea has also been used to reduce graphene oxide and develop some nanostructures that are targeted towards colon cancer cells, which showed almost two orders of magnitude more efficiency than previously tested graphene materials [54]. Glucose has also been used to reduce graphene oxide and prepare sheets in the presence of a Fe catalyst, developing a material that required 12 min to destroy cancer cells after being irradiated with an infrared laser source at a low concentration ( $0.05 \text{ mg mL}^{-1}$ ) [55].

Focusing on biotemplating, Xue et al. [56] developed gold nanoshells from an adenovirus vector after being co-incubated with  $\text{AuCl}_3$ . Apart from showing no significant cytotoxicity (minimum and maximum biocompatibility of 88.3% and 94.5%, for concentrations of  $2.5 \times 10^{-5} \text{ mM}$  and  $2.5 \times 10^{-4} \text{ mM}$ , respectively), these nanoshells led to the total death of tumoral cells in photothermal therapy using a light irradiation of  $4 \text{ W cm}^{-2}$ . Another study carried out by Shukla et al. [57] evaluated the impact of aspect ratio on biodistribution through cancer cells using components of tobacco mosaic virus as templates. They produced nanoparticles with different values for that aspect ratio, some of them labeled with polyethylene glycol (PEG) and others with the tripeptide RGD (Arg-Gly-Asp). After different histological analyses had been conducted, the researchers found that the PEGylated nanoparticles with the lowest aspect ratio (AR 3.5) diffused better into the tumor. Also, RGD-labeled nanoparticles were able to specifically interact with the endothelium of blood vessels, although they were rapidly cleared by immune cells. Therefore, these nanoparticles can be used as capsules for drug delivery as their behavior and functionality can be easily controlled [57]. Another study showed that PEGylated nanoribbons destroyed approximately 72% of a tumor after 24 h in the dark, without being toxic in a concentration of  $1 \text{ mg mL}^{-1}$  [58].

Drug delivery with hydrogels and aerogels is also being studied. Omid et al. [59] developed some graphene and chitosan and cellulose-based hydrogels to release an anticancer drug when receiving an external pH change from 7.4 to 5.4. Drug release studies were carried out with antimicrobial investigations which suggest that chitosan-based graphene hydrogels can act as promising drug delivery systems for different diseases. Also, some graphene aerogel nanoparticles were developed in acidic conditions and showed an effi-

cient pH-dependent release of drugs, and thus the authors suggest that these nanoparticles might be promising for tumors that develop in acidic media [60].

### 2.3. Bone Tissue Engineering

Inorganic polymers that are currently used as scaffolds in bone tissue engineering have been reported to have some drawbacks like cytotoxicity and limitations on recreating the 3D natural structure of bones [61]. Scaffolds for bone tissue engineering need to be porous and show some properties like osteoconductivity, biodegradability and bioactivity to avoid cells deposition and tissue formation on the edges of the scaffold [62,63]. To try and solve these drawbacks, bone tissue engineering using biotemplating to fabricate scaffolds has become an interesting approach to repair damaged tissue due to the structure of natural composites.

As hydroxyapatite is one of the main inorganic components that forms bones, synthesizing it from natural materials has been of great interest in this field. Despite its poor mechanical properties, it has good biocompatibility and osteoconductivity. Also, when hydroxyapatite is structured into different nanoshapes, its ability to act as bone filler is improved due to size. In 2010, Kim et al. [64] developed a hydroxyapatite nanotubular mesh using poly( $\epsilon$ -caprolactone) as a template. The results showed that the hydroxyapatite nanotubular mesh obtained could be readily applied as a filler for bone regeneration [64]. Also, a nanocomposite porous scaffold of tricalcium phosphate and hydroxyapatite nanofibers was developed. The toughness of the scaffold, evaluated by the area under the curve of stress displacement obtained in the compression tests, increased with the concentration of hydroxyapatite (from 1.00 to 1.72 kN m<sup>-1</sup>, as the concentration of hydroxyapatite increased to 5 wt.%) and showed better mechanical properties than previous calcium scaffolds [65].

The template used in a previously mentioned paper, poly( $\epsilon$ -caprolactone) (PCL), is a biodegradable and noncytotoxic [66] artificial polyester that is currently used as scaffold despite its poor cell affinity and hydrophobicity [67]. Considering both the advantages and limitations that hydroxyapatite and PCL offer, developing a material with both components may be useful for bone engineering. Qian et al. [67] produced a honeycomb-like PCL/nanohydroxyapatite from cane. These scaffolds showed the ability to support MG-63 cells adhesion, a cell line isolated from human osteosarcoma. PCL/hydroxyapatite composites were synthesized by an easy sol-gel synthesis method. The product obtained showed no sign of cytotoxicity and cells were able to proliferate and grow on these porous scaffolds, which made them promising scaffolds for bone tissue engineering. The incorporation of hydroxyapatite resulted in a better biocompatibility (approximately 30% increase as measured by tetrazolium-based colorimetric assay); this could be accounted for by the enhancement of cell attachment and protein adsorption on the scaffolds. Cane was also the template this group used in two different studies focused on the identification of new scaffolds for bone tissue engineering. One of them had the main objective of developing hydroxyapatite ceramic scaffolds using both biotemplating and the sol-gel method. When compared with pine-derived hydroxyapatite ceramic scaffolds, cane-derived scaffolds showed improved porosity (76–84% vs. 69–77% in pine-derived solids for sintering temperatures in the 1400–1100 °C range), which makes them more suitable for tissue engineering [62]. Another study focused on producing silk fibroin scaffolds from cane that provided an appropriate substrate for MC3T3-E1 cells, osteoblasts isolated from mice [68]. The biocompatibility, strength, and toughness of the silk fibroin protein make it a very interesting material for tissue engineering. The scaffolds exhibited good mechanical stability (compressive modulus of 1.56 ± 0.06 MPa), porosity (82.7%), and a bimodal pore size distribution (15 and 172  $\mu$ m).

Glass-ceramics can also be used in bone regeneration as they have been shown to induce the correct organization of a bone-like apatite layer on their surface. To prepare these glasses using a sustainable process of biotemplating, Qian et al. used sugarcane as a pattern to produce and characterize a biomorphic 45S5 bioglass [63]. Poly-L-lysine with a large positively charged surface for binding [69] has also been used for creating bioinspired

bone-tissue engineering materials. Gold colloids were deposited on poly-L-lysine coated fused silica to grow silicon nanowires with a controlled diameter. After 4 weeks, osteoblasts were differentiating and clustered on the surface, which suggests that these materials may have the potential to be applied in bone tissue engineering.

As has been previously mentioned, graphene has some properties like biocompatibility and conductivity that make it useful in photothermal therapy or drug delivery. Also, its capacity of promoting cell adhesion makes it appropriate for tissue engineering. Graphene nanogrids were used as templates for the proliferation of human mesenchymal stem cells. When there were some chemical inducers (dexamethasone,  $\beta$ -glycerophosphate, and ascorbic acid) these grids allowed for the fastest osteogenic differentiation of cells that had been reported, as they only took 7 days to achieve this process [70].

Recently, cellulose, alginate, bioglass nanoparticles, and gentamycin nanocomposite thin films were synthesized by electrophoretic deposition under different pressure conditions. Those that were prepared under a 5-bar pressure process showed more biocompatibility and improved osteoblast proliferation [71].

The regeneration of nervous tissue is another important approach in tissue engineering. It has been observed that, due to the electrical properties of graphene [72,73], its use in the nerve stimulation of neurons could be of great help to promote this regeneration. Different studies have been carried out using graphene oxide foams [72], fluorinated graphene [74], red ginseng-reduced graphene oxide [73], and graphene nanogrids on a SiO<sub>2</sub> matrix with TiO<sub>2</sub> nanoparticles [75]. General results showed that these materials were effective in inducing neural stem cells differentiation into neurons due to their ability to transmit electric currents that stimulate stem cells to become neurons, and the fact that they can express nestin, a neural marker. These characteristics show that these graphene-based materials may have a potential application in regenerative medicine.

Finally, it is important to highlight the role of viruses as templates for developing scaffolds and materials that could be used in tissue engineering. Specifically, plant viruses, such as tobacco mosaic virus, are of great importance in this field due to their inability to develop human infections, homogeneous pore distribution, and self-assembly capacity. Furthermore, they have a capsid that is extremely useful for nanomaterials synthesis on the inside, and that allows for genetic modification to achieve the desired morphology and functionality of the material. As this virus is stable at pH 2.5–9.0 and temperatures up to 90 °C and can also resist the presence of many organic solvents, tobacco mosaic virus is a potential template for tissue engineering [76–78].

#### 2.4. Light-Emitting Materials

The ability of living organisms to emit light, bioluminescence, can be used as a potential imaging tool. The most well-known light emitting mechanism that has been described is observed in fireflies, but isolating some of the molecules that participate in it is rather arduous. Recreating some inorganic materials based on luciferin, the substrate of the enzymatic reaction through which fireflies produce light, has been the focus of some studies related to this topic. A molecular lantern of gold nanoclusters decorated with green emitting dye ( $\lambda = 520$  nm) was synthesized with hydroquinone and dipeptide Cys-Gly. Due to good biocompatibility (98.4% of HeLa cells were alive after 24 h in the presence of the lantern even at high concentrations of 200  $\mu$ M), these materials have been proposed as promising imaging probes [79].

Optoelectronics is a field that needs constant improvement to meet the security and usefulness requirements of new devices. Some of these optoelectronic semiconductor materials like ZnO are capable of emitting light efficiently in ambient conditions. To develop a sustainable process of synthesizing ZnO semiconductor materials using biotemplating, rattan was used as a template. Al<sub>2</sub>O<sub>3</sub> microvessels were produced and coated with ZnO tetrapods. The intensity of the emission that can be easily controlled and the internal structure of the bioinspired material make them a potential candidate for a semiconductive optoelectronic material and a gas sensor composite, respectively [80].

Also, porous ceramic burners have shown high efficacy in producing light and heat sustainably to promote a green economy. Yttrium disilicate ( $Y_2Si_2O_7$ ) is a rare earth disilicate that is stable at high temperatures and has a luminescent performance. These materials exhibit light emission in the infrared range ( $\lambda = 750\text{--}4300\text{ nm}$ ) and at the wavelength of  $1000\text{ nm}$  at  $400\text{ }^\circ\text{C}$ . Santos et al. [81] developed  $\beta\text{-}Y_2Si_2O_7$  from the sponge *Luffa Cylindrica*, which showed good gas burning and light emission efficiency. Using the same template and product, they obtained a dysprosium-doped yttrium disilicate burner with a micro-porous structure and thermoluminescent response at  $580\text{ nm}$  at  $180\text{ }^\circ\text{C}$ . The prepared material showed a porous microstructure and a pycnometric density of  $3.21\text{ g cm}^{-3}$  (80% of the theoretical value density, which accounts for  $4.04\text{ g cm}^{-3}$ ), which suggests that biotemplating allowed for the synthesis of morphology-controlled structures with good burner efficiency [82].

### 2.5. Sensors

Tin dioxide ( $SnO_2$ ) is highly used in the development of gas sensors as it is a cost-effective semiconductor with chemical stability. The process through which the gas is detected takes place on the surface of the nanomaterial, between the desired target gas and the oxygen of  $SnO_2$ . Therefore, porosity is essential to ensure the presence of channels for gas diffusion [83,84]. Zhu et al. took advantage of the porous hierarchical structure of *Euploea mulciber* butterfly wings to create PdO-decorated  $SnO_2$  nanocrystallites with a high sensitivity of 229 (to 200 ppm acetone) and rapid response/recovery time of 10 s/31 s (to 50 ppm acetone) at  $230\text{ }^\circ\text{C}$ . This sensitivity and rapid response/recovery might be caused by the size and hierarchical structure of nanoparticles, which promote gas diffusion through them [84]. Also,  $SnO_2$  crystal films have been produced using cellulose crystals as templates. The final product was a fast (approximately 3 s until 90% of the maximum signal) and highly sensitive (at ppm levels) sensor to carbon monoxide and showed better performance than other CO sensors described in the literature, which took, for example, 10 s to several minutes until 90% of the maximum signal was achieved [83].

Pressure and strain sensing have emerged in the last few years due to their applicability to the manufacture of wearable electronic devices. The focus of producing new pressure sensors is improving their sensitivity and detection limit. To achieve that, wrist pulse pressure sensors with polypyrrole layers produced from the replication of rose petals have been developed. They exhibit an ultrahigh sensitivity ( $70\text{ KPa}^{-1}$ ,  $<0.5\text{ KPa}$ ), an ultralow detection limit ( $0.88\text{ Pa}$ ), a wide pressure detection range (from  $0.88\text{ Pa}$  to  $32\text{ KPa}$ ), and a fast response time (30 ms). Moreover, upon light illumination, sensitivity enhanced to  $120\text{ KPa}^{-1}$  ( $<0.5\text{ KPa}$ ) and the detection limit lowered to  $0.41\text{ Pa}$ . Due to the petal structure, the pressure sensors were capable of showing excellent sensing activity [85]. A similar observation was made in the development of an engineered-Au/poly(dimethylsiloxane) strain sensor using a lotus leaf as a template. The results showed that the strain sensor had a high sensitivity (gauge factor = 20 at 20% strain, 350 at 80% strain) and a wide sensing range (up to 80%), being able to detect subtle strains like human wrist pulse [86].

Also, biotemplating has been used to prepare a high resolution optical fiber surface-enhanced Raman scattering sensor using cicada wings [87]. These templated materials were coated with silver and their functionality was tested with thiophenol and rhodamine 6G as analytes. Authors obtained the characteristic thiophenol peaks that are described in the literature ( $1573\text{ cm}^{-1}$ ,  $1071\text{ cm}^{-1}$ ,  $1021\text{ cm}^{-1}$ ,  $1000\text{ cm}^{-1}$ ,  $692\text{ cm}^{-1}$ , and  $422\text{ cm}^{-1}$ ) and the characteristic rhodamine 6G spectra but with a broad silica peak at  $400\text{ cm}^{-1}$  due to the experimental conditions that they used to analyze this compound. The fidelity and sensitivity obtained by these results show the potential application of these materials in sensing. Photonic crystals for temperature and gas sensors from *Entimus imperialis* beetle scales and a mixture of organopolysiloxane were prepared [26]. The silica-based replica of these scales could resist temperatures up to  $600\text{ }^\circ\text{C}$ . Authors suggest that changing structural characteristics of organopolysiloxane could allow for the synthesis of sensors



with tunable properties and therefore materials with the desired photonic characteristics could be prepared.

Electrophoretic deposition was used to develop some graphene oxide nanowalls which were effective in the detection of single nucleotide polymorphisms of a DNA determined sequence. This is of great interest as they can be used as biosensors with high sensitivity in detecting mutations that could lead to diseases like cancer and help in their prevention [88]. In fact, graphene-based technologies, while being less expensive, showed a five orders of magnitude higher detection sensitivity of leukemia cells than reference technologies such as next generation sequencing of DNA [89].  $Mg^{2+}$  charged graphene electrodes fabricated by electrophoretic deposition also showed more efficiency and a lower detection limit (about 1000 orders of magnitude) than conventional techniques in detecting leukemia cells in a fast period of 60 min, with the advantage of requiring less investment and incubation time [90].

Copper oxide nanoflakes were synthesized to act as biosensors for the detection of *E. coli* [91]. These structures were reduced by hydrogen produced during the glycolysis process of the bacteria to become active, which makes them suitable for detecting all types of bacteria that carry out this process. It showed high sensitivity as it was able to detect low concentrations of bacteria of  $10^2$  CFU  $mL^{-1}$ . Another study showed that bacterially reduced graphene oxide by hydrogen produced in that glycolysis process exhibited antibacterial activity inhibiting bacteria proliferation on its surface. These findings suggest that reduced-graphene oxide can be used to develop thin coatings to inhibit bacterial proliferation in specific areas [92].

Finally, it is important to highlight commercial applications of biotemplated sensors. Some sensors were developed to be used in the food industry to detect fish freshness using rape bee pollen as a template [93]. The sensor was based on the fluorescence quenching of ZnO by  $H_2O_2$  produced by xanthine oxidase in the oxidation of xanthine, a molecule that helps in fish freshness detection. The prepared sensor was able to detect low concentrations of xanthine, with a limit of detection of  $1.3 \times 10^{-10}$  mol  $L^{-1}$ , which suggests that the synthesized material is accurate in determining fish freshness and that of other high-protein foods.

## 2.6. Energy Capture and Storage

The development of Li batteries has been of significant importance in recent years as they are the main candidates for next generation energy storage due to their capacity and cost effectiveness. However, there are still some limitations related to safety when it comes to their use in large electronic devices. To improve the internal resistance of the batteries using nanosized and intricate structures of natural materials to decrease the path that electrons have to travel, and thus reduce the heat that damages batteries in high thermal resistance materials, biotemplating has been widely used in the synthesis of useful materials not only for its ability to control the morphology of the product but also because it allows for an environmentally friendly synthesis process [94]. There are different types of Li batteries for which bioinspired materials have been synthesized, like Li-S, Li-Se, or Li-oxygen. Also, biotemplating has been useful to develop suitable materials for energy harvesting applications [95], supercapacitors, solar cells, and Na batteries.

Producing  $FeS_2$  bioinspired materials was the focus of the study developed by Gan et al. in 2016, because this metal sulfide has been considered a useful anode material for its low environmental impact. Using cotton as a template and a carbon source, they developed high capacity  $FeS_2$  decorated sulfur-doped fibers that were applied as the anode of Li batteries [96]. Specific capacities were about 1200, 900, 700, 550, and 400 mAh  $g^{-1}$  after every 10 cycles at 0.1, 0.2, 0.5, 1, and 2 A  $g^{-1}$ . Mirvaux et al. [97] produced other iron-based electrodes for Li batteries by using the bacteria *Sporosarcina pasteurii* as a nucleating template. Bacteria played different roles such as a template for the growth and organization of particles, a source of carbon residue (beneficial to electrode conductivity), and a source of porosity (which favors lithium ions mobility) because of gas released upon mild heating to

decompose bacteria. The resulting electrode materials exhibited enhanced performance (in terms of first cycle reversibility, reversible capacity, power efficiency, and cycle life) as compared to similar solids obtained without the use of bacteria biotemplating.

Further progress in Li batteries requires the substitution of graphite as negative electrode materials in those devices with other composites, including  $\text{TiO}_2$ ,  $\text{RuO}_2$ , or  $\text{IrO}_2$  [98], that have demonstrated a low environmental impact and a higher capability than graphite, apart from being safer and faster. Using  $\text{TiO}_2$  nanostructures for this matter enhances the effectivity of batteries because of the increase in electrode–electrolyte contact area. Taking this into account, hollow  $\text{TiO}_2$  nanofibrils from nanofibrillated cellulose were synthesized through a biotemplating technique [99]. Despite replicating the structure of cellulose, the performance of the material was not impressively improved. However, this shows a potential approach to produce  $\text{TiO}_2$  electrodes for Li batteries. Kim et al. [100] used diphenylalanine as a template to design a hollow ribbon anatase  $\text{TiO}_2$  nanonetwork structure to be used as an electrode for Li batteries through biotemplating and an atomic layer deposition technique. This unique structure provides the material with some advantages like facile electronic conduction and better performance than previous nano-electrodes due to an improved Li diffusion. These nanoribbons showed a  $154.5 \text{ mAh g}^{-1}$  capacity and retained 83.2% of the initial capacity after 200 cycles, which is much higher than that obtained by  $\text{TiO}_2$  nanopowder, which accounted for a  $73.5 \text{ mAh g}^{-1}$  specific capacity, retaining 68.8% of it after 200 cycles.

Also, some metal oxide–graphene materials have been used to improve the cycling life capacity of conventional carbon anodes.  $\text{SnO}_2/\text{C}$  composites were developed by Li et al. in 2014 from cotton, due to its plant fibers' uniform morphology. The final product had a higher reversible capacity ( $530 \text{ mAh g}^{-1}$ ) than carbon anodes ( $372 \text{ mAh g}^{-1}$ ) [101]. Other examples of metal oxide–graphene anodes were developed by Ping et al. [102], where genetically modified *E. coli* to express 5R5 proteins on its surface was used as a template to develop rod-shaped mesoporous silica particles, as 5R5 is a protein that is integrated by five repetitions of the R5 domain. This domain is responsible for the catalytic activity of a protein that can synthesize silica in vitro, called silaffin. Tetraethyl orthosilicate was the  $\text{SiOx}/\text{C}$  precursor. These nanorods showed a specific capacity of  $791.7 \text{ mAh g}^{-1}$  after 100 cycles, higher than that of non-templated  $\text{SiOx}$  ( $\sim 400 \text{ mAh g}^{-1}$ ) [102]. In another study,  $\text{NiO}/\text{C}$  microspheres were synthesized by biotemplating using lotus pollen grains as both a template and a carbon precursor in a chemical bath deposition method [103]. In using  $\text{NiO}/\text{C}$  microspheres as an anode material for Li batteries, a high discharge capacity and stability (after 10 cycles, the specific capacities at 0.1, 0.5, 1, and  $3 \text{ Ag}^{-1}$  were 698, 608, 454, and  $352 \text{ mAh g}^{-1}$ , which were 88.4–98.7% of the initial capacities) were achieved [103]. Sea cucumber-like  $\text{LiMn}_2\text{O}_4/\text{C}$  composites were synthesized through a biotemplating technique by using spirulina as a template. These composites showed improved electrochemical performance ( $130 \text{ mAh g}^{-1}$  after 10 cycles compared to  $118 \text{ mAh g}^{-1}$  of a  $\text{LiMn}_2\text{O}_4$  obtained by a sol-gel method), which could be related to its hierarchical structure, as it could facilitate lithium-ion conduction and slow down magnesium dissolution in electrolytes during the performance of the battery [104]. Another metal oxide–graphene high-capacity electrode was developed using spirogyra as a template and as a carbon source in the study conducted by Wang et al., where they designed a  $\text{MnO}/\text{C}$  anode for lithium batteries [105]. These electrodes exhibited high reversible lithium storage capacity ( $610 \text{ mAh g}^{-1}$  at  $200 \text{ mA g}^{-1}$ ) [105]. This metal oxide had also been used in the past to develop microspheres as electrode materials from *Nannochloropsis oculata* for Li batteries, with a high reversible capacity of  $700 \text{ mAh g}^{-1}$  at  $0.1 \text{ A g}^{-1}$  and a cycling stability of 94% capacity retention [106]. Xia et al. developed  $\text{LiFePO}_4/\text{C}$  composites from spirulina to serve as a high potential cathode for lithium ion batteries which showed an excellent cycling stability of  $141 \text{ mA g}^{-1}$  after 50 cycles [107]. Also, some studies have shown a specific binding capacity of some polypeptides depending on the amino acids sequence to cathode materials, such as the previously mentioned  $\text{LiMn}_2\text{O}_4$  or  $\text{LiCoPO}_4$ , which might be useful to improve their potential theoretical value, poor cyclability, and rate capability [94].

Sugarcane bagasse has been used to design single-crystalline  $\alpha$ - $\text{MoO}_3$  micro belts with high electrochemical performance ( $302 \text{ mA g}^{-1}$  and  $99.4 \text{ mAh g}^{-1}$  at  $100 \text{ mA g}^{-1}$  and  $2000 \text{ mA g}^{-1}$ , respectively) and discharge capacity ( $270 \text{ mAh g}^{-1}$  after 200 cycles) [108]. In addition, Zhu et al. produced MnO/C porous composites with hollow structures from lotus pollen grains by combining biotemplating with chemical bath deposition. These composites showed an excellent cycling stability ( $740 \text{ mAh g}^{-1}$  after 50 cycles) which makes them a potential anode material for Li batteries [109].

In addition, to improving the capacity and stability of graphitic carbon anodes, silicon oxycarbides (Si–O–C) have received great attention. Xia et al. [110] developed Si–O–C microspheres as an anode material for Li batteries by using *Nannochloropsis* microalgae as a template and a carbon source and supercritical  $\text{CO}_2$  fluid technology to assure high penetration and mass transfer control into the pattern. The product showed a high reversible capacity of  $450 \text{ mAh g}^{-1}$  (compared to  $248.9 \text{ mAh g}^{-1}$  of carbon) and a higher cycling stability ( $453.5 \text{ mAh g}^{-1}$  after 200 cycles at  $0.1 \text{ A g}^{-1}$ ) than carbon electrodes, which suggests that using both biotemplating and supercritical  $\text{CO}_2$  fluid technology will produce useful materials in a sustainable and controllable way. In fact, they used these two processes to synthesize  $\text{Ni}(\text{OH})_2$  modified porous carbon microspheres from yeast to serve as cathodes, with a high discharge capacity ( $1335 \text{ mAh g}^{-1}$  at  $0.1 \text{ C}$ ) and good cycling stability ( $602 \text{ mAh g}^{-1}$  after 200 cycles) [111]. Other Si–O–C composites have been developed using those two techniques, resulting in the production of cathodes that not only encapsulated Se in Li–Se batteries, but also showed a high capacity and cycling stability [112].

Reducing the temperature of the synthesis process of garnet solid state electrolytes materials to lower lithium evaporation is another major objective. This was achieved through a sol-gel method, by creating high conductivity tetragonal  $\text{Li}_7\text{La}_3\text{Zr}_2\text{O}_{12}$  and cubic  $\text{Li}_{6.4}\text{Al}_{10.2}\text{La}_3\text{Zr}_2\text{O}_{12}$  using Agar polymer due to its low cost [113]. The authors hypothesized that this decrease in the temperature synthesis process might be attributed to a homogeneous metal ion mixing and garnet nucleation in the templated matrix.

Lithium–sulfur batteries attract great attention as a more energetic option than normal lithium batteries. In the work of Xia et al. [15], porous carbon microspheres were prepared by using *Schizochytrium sp.* microalgae. These particles did not only show high reversible capability and good cathode properties, but could also encapsulate sulfur to reduce the degradation of electrodes in Li–S batteries due to the accumulation of lithium polysulfides [15]. Reducing this effect, which is called the “shuttle effect”, is essential to improve the performance of Li–S batteries. Kong et al. [114] fabricated aluminum-doped ZnO nanoparticles-decorated carbon nanoflakes decorated using kapok fibers as templates. Owing to their electrochemical performance (initial discharge capacity of  $1114 \text{ mAh g}^{-1}$  and  $927 \text{ mAh g}^{-1}$  after 100 cycles), these nanoparticles demonstrated a reduced shuttle effect and improved the performance of Li–S batteries [114]. Also, this template was used to develop carbon nanoflakes decorated with metal oxides nanoparticles. The application of  $\text{MgO}/\text{C}$ ,  $\text{La}_2\text{O}_3/\text{C}$ , and  $\text{CeO}_2/\text{C}$  as sulfur cathodes showed a higher capacity ( $1.368 \text{ mAh g}^{-1}$ ,  $1.345 \text{ mAh g}^{-1}$ , and  $1.388 \text{ mAh g}^{-1}$ , respectively) and cycling stability (0.034%, 0.047%, and 0.066% capacity decay per cycle, respectively) than  $\text{Al}_2\text{O}_3/\text{C}$  and  $\text{CaO}/\text{C}$  electrodes ( $1.330 \text{ mAh g}^{-1}$  and  $1.246 \text{ mAh g}^{-1}$ , respectively). Also,  $\text{CaO}/\text{C}$  showed a poorer lithium polysulfides capture capability in reducing the shuttle effect than  $\text{MgO}/\text{C}$ ,  $\text{La}_2\text{O}_3/\text{C}$ , and  $\text{CeO}_2/\text{C}$  because, as those sulfides are poor ionic and electronic conductors, they are better captured by electrodes with a better cycling performance [115]. They also developed some Sn@C composites to serve as anodes for Li batteries using the microalgae *Spirulina platensis*, as metallic tin is an interesting option for anodes material due to its theoretical capacity ( $993 \text{ mAh g}^{-1}$ ), its high operating voltage, and its resistance towards solvent that minimizes irreversible charge loss [116]. In another study, *E. coli* was coated with metal–organic frameworks to manufacture N and P co-doped carbon capsules to express self-phosphorized metal phosphides. Owing to the dispersion of these particles over the bacteria carbon capsule, they can bind to lithium polysulfides and therefore suppress

polysulfide shuttling. They can also catalyze oxygen conversion, which makes them a great material for lithium–sulfur batteries and zinc–air batteries [117].

To produce lithium–cobalt batteries, Kang et al. [19] developed the biotemplating technique using wood, cotton, and pollen as templates. Due to the performance of the final product and its potential for commercialization, cotton was selected as the appropriate pattern among the ones they tested. Cotton–Li–Co batteries showed a higher capacity ( $52.6 \text{ mAh g}^{-1}$ ) than traditional ones ( $36.2 \text{ mAh g}^{-1}$ ).

Porous structures in gas batteries are desirable to achieve improved gas access, and therefore improved performance efficiency. In this respect, producing porous materials with controlled pore sizes through biotemplating provides an easy process to synthesize useful materials in a sustainable form. In Li–oxygen batteries, the solid/gas interface of the cathode is crucial, so having porous structures to facilitate the entrance of the gas will allow a much more extended use of these batteries, which are considered to have three times more energy density than Li batteries. Oh et al. [118] used different non-pathogenic bacteria (*E. coli* and *S. epi*) to prepare cathode materials with pores of 200–500 nm to 1–2  $\mu\text{m}$  size and geometrical shapes including cylindrical and spherical ones. The porous multiwalled carbon nanotubes obtained were more beneficial when the pores were cylindrical (produced by *E. coli*), showing more power and an improved cycle life than spherical pores ( $3.46 \text{ mAh g}^{-1}$  compared to  $2.73 \text{ mAh g}^{-1}$  of *S. epi* multiwalled carbon nanotubes; and 2–3 times more total discharge capacity, respectively). The authors suggested this might be attributed to the better interconnectivity of cylindrical pores.

Supercapacitors are energy storage devices with long life cycle and high power. In 2015, based on the extremophile bacteria *Deinococcus radiodurans* as a biotemplate, Atalay et al. [119] used  $\text{NiCl}_2$  as a precursor to produce NiO nanostructures with a high surface-to-volume ratio for synthesizing potential materials for supercapacitors. Sawdust was used as a template to fabricate porous  $\text{Co}_3\text{O}_4$  nanoparticles, as it is a low-priced and abundant material. They showed strong reversibility, high capacitance, and stability ( $179.1\text{--}289.7 \text{ F g}^{-1}$  at 20 mA after 100 cycles), which made them appropriate for a supercapacitor [120]. Cellulose nanocrystals from cotton were used to produce orthorhombic niobium pentoxide nanocrystalline films with lithium-ion intercalation pseudocapacitance. The material exhibited good cycling performance, wide temperature tolerance, and a unique intercalation capacity that provide an interesting approach for the production of materials with high power and energy density for energy storage [121]. The black wings of *Troides Helena* butterflies were used as a pattern for the synthesis of biomorphic NiO/Ni supercapacitor electrode materials with a higher capacitance and stability than non-templated materials ( $381.4 \text{ F g}^{-1}$  at  $1 \text{ A g}^{-1}$  compared to  $251.2 \text{ F g}^{-1}$  at  $1 \text{ A g}^{-1}$  for non-templated NiO). The wings were correctly replicated as can be seen in Figure 2, although pores in the structure were reduced and ridges achieved a serpentine shape compared to the original template [25]. Mycelium pellets [122] and polyalanine [123] have also been used to prepare useful materials for the production of supercapacitor devices.

Biotemplating has also been used to develop electrodes from different templates such as viruses [17,124–126], proteins [127], and plants [128] for different applications. For example, it has provided the solution for a global problem involving a lack of potable water. One of the most relevant techniques is deionization, where ions in water are attracted towards electrodes with a potential difference, causing a diminished concentration of these ions in water. Bioinspired materials including carbon electrodes derived from rattan have been applied to water desalination. These materials showed excellent performance in adsorbing high concentrations of salt ( $\sim 0.058 \text{ g}$  of salt from a  $10 \text{ g L}^{-1}$  salt solution) by applying a voltage as low as 1.2 V [128].

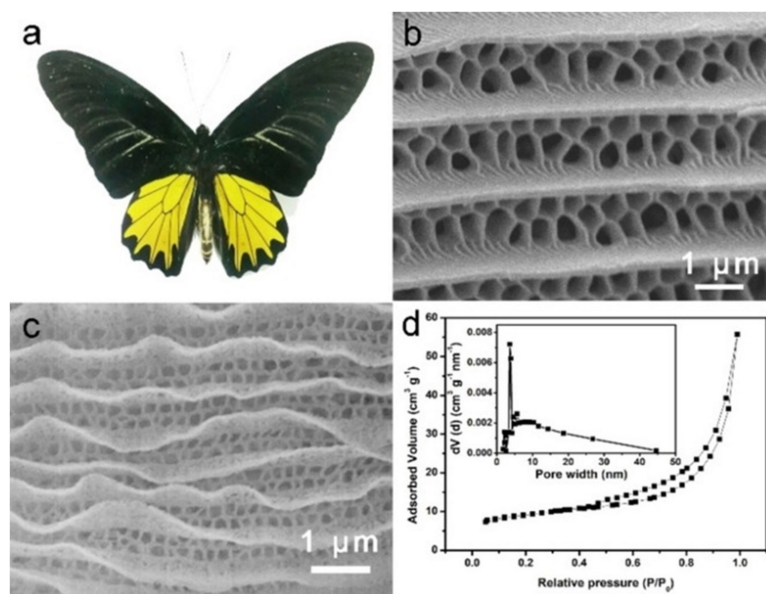


**Figure 2.** Figure extracted from Tong et al. (2021) [26]. Picture (a) shows an image of the *Troides Helena* butterfly used as a template. Pictures (b,c) compare the original template and the templated material, respectively. Although the structure was accurately replicated, pores diminished their sizes and ridges changed their straight disposition. Picture (d) shows nitrogen adsorption/desorption isotherm and pore size distribution of the biotemplated electrode. Reproduced with the permission of Wiley.

Solar cells are electronic devices that can transform light into electric energy. There is an urgent need to improve the performance of solar cells, including their light absorption capability and carrier transport. One of the main strategies to achieve this is to synthesize materials with nanoscale architectures, which improves charge collection and light harvesting with the incorporation of different metals on their active layer. As natural materials have a highly porous structure and intricate nanoscale hierarchy, using biotemplating to solve this matter is of great interest. Dorval et al. [129] designed solar cells through biotemplating of M13 bacteriophage to produce titania–lead sulfide heterojunctions that were also complexed with gold and silver nanoparticles and nanoplates. They obtained a 36.5% improvement in power conversion efficiency (measured as the percentage of solar light converted into electrical energy) using virus-based devices with silver nanoplates compared to that obtained by virus-based devices without nanoparticles. Another group [130] applied an entangled hollow  $\text{TiO}_2$  nanoribbon anode from diphenylalanine for dye-sensitized solar cells that showed a power conversion efficiency of 3.8%, which is comparable to that obtained by commercial titania (3.5%) [130]. *Sasakia Charonda Formosana* butterfly wings were also used for the preparation of  $\text{TiO}_2$  nanocrystal solar cells [131].

Na batteries are considered an alternative to Li batteries due to the abundance and the low cost of sodium; therefore, developing bioinspired materials for this application is attracting attention. The M13 bacteriophage was chosen by Zhang et al. [132] to develop zinc sulfide nanofibers coated with a layer of carbon to serve as anodes for Na batteries. It is necessary to find high-capacity anode materials for sodium batteries as sodium ions are not able to intercalate into conventional graphite anodes. Although the product showed good reversible capacity and efficiency ( $603 \text{ mAh g}^{-1}$  at  $100 \text{ mA g}^{-1}$  discharge rate), the authors suggested that more research was required to reduce the production cost [132]. Dextran has also been used with this purpose. Using this template allowed the authors to control the morphology of the nanoparticle, which exhibited a higher energy storage capacity than traditionally created materials after the same conditions ( $103.1 \text{ mAh g}^{-1}$  compared to  $80.1 \text{ mAh g}^{-1}$  after 10 cycles, respectively) [133].

## 2.7. Catalysis

### a) Sustainable production of hydrogen and biofuel

The current energy system is based on fossil fuels. As their combustion releases polluting elements that contribute to climate change, finding renewable and sustainable energy sources is essential to reduce those damages to the environment. The replacement of these fossil fuels using biomass-derived alternatives has taken a substantial leap towards a sustainable energy system to meet the global growing demand. In 2017, Xue et al. [134] developed a biorefinery process to co-produce biofuels and silver nanomaterials. Impregnation of pure cellulose with silver nitrate and subsequent pyrolysis led to a substantial increase in gas yield (especially hydrogen, three times higher than using raw cellulose) and higher content in furfurals (e.g., 5-hydroxymethylfurfural content is doubled) of the condensable biooil components. Moreover, the authors suggested that the silver-char components be calcined to yield biotemplated silver nanomaterials for use in catalytic energy applications. Another approach towards a sustainable biofuel production process was assessed in 2020 by Ashman et al. [135]. Impregnation of silver nitrate into the spent grain waste of a brew through a wet impregnation method prior to pyrolysis resulted in a dramatic increase in non-condensable gas production (hydrogen and ethane, a 10-fold increase in the case of the former). Moreover, fuel production was accompanied by the biotemplated synthesis of micro- and nanostructured materials.

Hydrogen is an attractive alternative to fossil fuels since water vapor is the only product obtained through its combustion. However, it is currently mainly obtained from natural gas, oil, or coal. One alternative is hydrogen production from biomass-derived oxygenated organic compounds (photo-reforming) using light in the presence of water, at room temperature and anaerobic conditions, to generate gaseous hydrogen and carbon dioxide. The process uses a semiconductor as the catalyst that needs to be activated through light to complete its function. To be activated, the photon that is absorbed from light needs to have the same or higher energy than the difference between the conduction band and the valence band (band gap). Chen and Wang [136] designed boron carbon nitride tube catalysts from kapok fibers which were used as a template and carbon source. The performance of the boron nitride tubes was evaluated in the production of hydrogen using triethanolamine as a sacrificial reagent and Pt as a cocatalyst under visible light, obtaining a hydrogen evolution rate of  $2.8 \mu\text{mol h}^{-1}$ . Hashemizadeh et al. synthesized biotemplated artificial titania leaves with the architecture of *Camellia* tree leaves [1]. Subsequent incorporation of ruthenium oxide on the surface resulted in a material able to reduce  $\text{CO}_2$  under UV and visible light. Results showed that these biotemplated catalysts had a higher selectivity for methane in the reduction of  $\text{CO}_2$  under UV light and an enhanced visible light activity than P25, a reference commercial titania photocatalyst (selectivity of  $3.8 \mu\text{mol}$  per grams of catalyst compared to  $5.1 \mu\text{mol}$  per grams of catalyst of P25, which yields mostly CO). This higher selectivity was attributed to the interconnected nanostructures that were achieved after replicating the thylakoid membrane of the leaves [137], as their hierarchical pore network increases the time that reactants are in contact with the titania surface of thylakoids, increasing the possibility of full  $\text{CO}_2$  reduction to  $\text{CH}_4$ . Other green leaves including olive leaves were used as templates to create a titania-based catalyst (artificial olive leaf, AOL) to participate in the production of hydrogen through glycerol photoreforming. As olive leaves and glycerol are by-products from olive oil and biodiesel production, respectively, their use as templates for catalysts and as a sacrificial agent, respectively, in photoreforming constitutes an interesting valorization route for biohydrogen production. AOL produced 64% and 144% more hydrogen than P25 and under solar light irradiation and UV irradiation, respectively. These results show the potential applications of olive leaves as a template for photocatalysis [21]. This catalyst was further tested after depositing copper on the structure. Results showed that both under solar light and UV light irradiation, copper enhanced the photocatalytic activity and therefore hydrogen production in glycerol photoreforming. This synergistic effect of titanium and copper was attributed to a heterojunction between  $\text{TiO}_2$  and  $\text{CuO}$ , where electrons accumulated at the  $\text{CuO}$  conduction band reduced protons

to hydrogen and holes in titania oxidized glycerol. However, a high quantity of copper deposited on the structure decreased the activity, probably as a result of copper acting as an electron–hole recombination center [138].

Cerium oxide ( $\text{CeO}_2$ ) has a high stability and efficient photocatalytic activity under UV radiation due to its wide band gap ( $\sim 3\text{--}3.2\text{ eV}$ ) [139], so it is considered a promising photocatalyst for hydrogen production reactions. To enhance its photocatalytic activity, N- $\text{CeO}_2$  has been used to extend the light absorption capability towards the visible light region and slow down the electron–hole recombination rate. Liu et al. [140] studied the application of N-doped hollow  $\text{CeO}_2$  spheres prepared from *Hemerocallis* pollen grains to hydrogen production through methanol photoreforming. These spheres, which completely replicated the natural structure of the template, acted as biotemplated catalysts that produced almost 4 times more hydrogen than  $\text{CeO}_2$  nanopowder ( $521\ \mu\text{mol h}^{-1}\text{ g}^{-1}$  vs.  $141\ \mu\text{mol h}^{-1}\text{ g}^{-1}$ ). This enhancement in the photocatalytic activity might be attributed to the fact that the introduction of nitrogen in the structure can maintain the hydroxyl groups on the surface of  $\text{CeO}_2$  to favor hydrogen production reaction (Figure 3) [140].

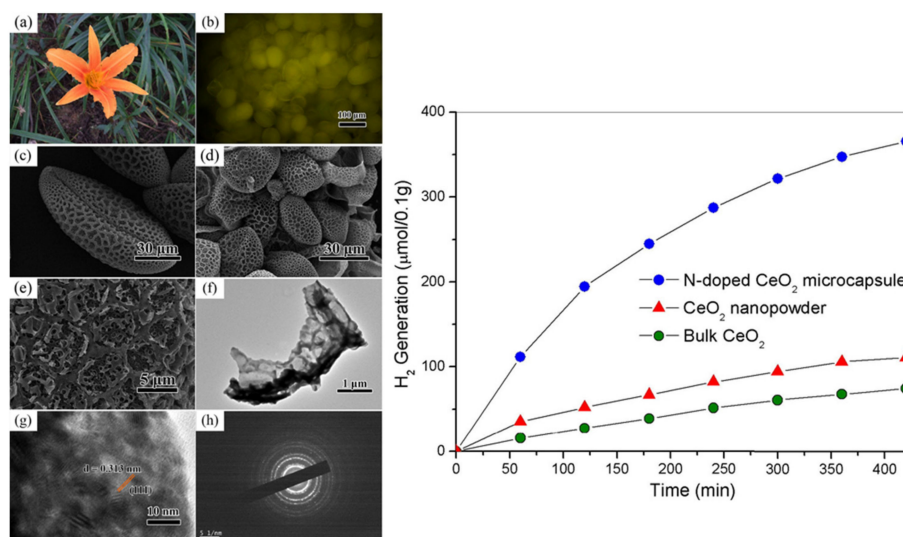


**Figure 3.** Figure extracted from Liu et al. (2017) [140]. Picture (a) is an image of the template *Hemerocallis fulva* and (b) is a fluoroscopy photograph of pollen. Pictures (c,d) show SEM images of both the original template and the templated material, respectively and (e) shows the porous surface of biotemplated  $\text{CeO}_2$  microcapsule at a lower scale. Pictures (f–h) show the TEM image of the templated  $\text{CeO}_2$  microcapsule, HRTEM image of the templated  $\text{CeO}_2$  microcapsule and the selected area diffraction pattern of  $\text{CeO}_2$  nanoparticles, respectively. The right picture also shows hydrogen production comparing the templated material (N-doped  $\text{CeO}_2$  microcapsules) with non-templated forms of  $\text{CeO}_2$ . Reproduced with the permission of Elsevier.

Strontium titanate has been used to produce hydrogen from water splitting, although its performance under visible light is limited due to its large band gap (indirect band gap of 3.25 eV and direct band gap of 3.75 eV) [141]. To address this problem, Nuraje et al. [142] prepared photocatalytically active N-doped perovskite strontium titanate ( $\text{SrTiO}_3$ ) nanowires from a genetically engineered M13 virus to produce hydrogen by water splitting under visible-light irradiation. Reactions were carried out by adding 0.05 g of strontium titanate to 60 mL of a mixture of methanol: water (1:1.4 v/v) under visible light using Pt nanoparticles as co-catalysts.  $\text{SrTiO}_3$  nanowires that were treated at 650 °C during the ammonia treatment showed the highest photocatalytic activity at producing  $\text{H}_2$  ( $40\ \mu\text{mol g}^{-1}\text{ h}^{-1}$ ). This result is significantly better than the hydrogen rate achieved by non-templated  $\text{SrTiO}_3$  described in the literature ( $\sim 10\ \mu\text{mol g}^{-1}\text{ h}^{-1}$ ) [143]. The improvement in hydrogen production by this templated catalyst can be ascribed to doping with N, which enhances solar light absorption [142].

## b) Decontamination reactions

Pollution is one of the main problems that mankind is facing. Photocatalysis is the main strategy used jointly with biotemplating to address this problem. Azmy et al. [144] designed BiFeO<sub>3</sub> nanoparticles to act as catalysts for the degradation of methylene blue under visible light irradiation, as their narrow band gap of 2.1 eV makes them a good material for visible light capture. The template they used was  $\kappa$ -carrageenan, a sulfated polysaccharide extracted from red seaweed that allows for the nucleation of nanoparticles. The results showed that 12.79 mmol/L of BiFeO<sub>3</sub> could degrade 10 ppm of methylene blue over a 120 min period and remove 96% of the dye at pH 8 in a 180 min period. They suggested that the adsorption capacity of the materials depends on the concentration of the dyes, and that BiFeO<sub>3</sub> is a better catalyst than an adsorbent, as in basic media it could not adsorb the dyes but it could catalyze methylene blue degradation. The reusability experiments the authors carried out showed that the catalyst did not lose activity until the third cycle. To catalyze the same reaction, Yang et al. produced hierarchical Fe<sub>2</sub>O<sub>3</sub>/C composites from agarose which showed enhanced photocatalytic activity with a four times higher photodegradation rate constant of 0.091 min<sup>-1</sup> vs. the 0.020 min<sup>-1</sup> rate constant of Fe<sub>2</sub>O<sub>3</sub> [145].

TiO<sub>2</sub> is another interesting semiconducting photocatalyst because of its nontoxicity, high activity under ultraviolet light, and low cost. Some TiO<sub>2</sub>-based photocatalysts were developed from *Juncus effuses* to be used in the degradation of water or gas pollutants. The results showed that the photocatalytic activity of the biotemplated photocatalysts in the degradation of methylene blue was better than that of P25, mainly due to the auto-doping of carbon into titania [146]. Ivanova et al. [147] designed some titania porous films using nanocrystalline cellulose from cotton as a template. The resulting material showed photocatalytic activity as well as excellent performance as thin anodes for dye-sensitized solar cells (they showed a current density of 6.02 mA cm<sup>-2</sup> compared to 5.24 mA cm<sup>-2</sup> of a reference titania cell). To demonstrate its photocatalytic activity, the material was used to purify aqueous media polluted by 4-chlorophenol. The degradation of 4-chlorophenol with the biotemplated films had a higher first-order rate constant (0.18 h<sup>-1</sup>) than the highest reported rate (0.12 h<sup>-1</sup>). It was also tested in the catalytic oxidation of NO, showing a conversion efficiency of 16% over the 10% obtained with previous catalysts. This behavior was attributed to the high crystallinity, porosity, and the presence of the anatase phase in the titania films [147].

However, fast recombination of TiO<sub>2</sub> electron-hole pairs needs to be assessed to improve its performance. To address this problem, doping with metals or non-metals and TiO<sub>2</sub>-carbon heterojunctions are some of the possibilities. C-doping of TiO<sub>2</sub> has been reported to improve its photocatalytic activity in the visible spectra while being more effective than other non-metal doping because it can enhance both TiO<sub>2</sub> conductivity and surface adsorption [148]. C-doped TiO<sub>2</sub> nanorods were developed using regenerated cellulose membrane from non-printed area of recycled newspaper, which served as both a template and a carbon source. The photocatalytic activity of these catalysts was analyzed through methyl orange degradation, to be used in reactions to purify polluted water. Results showed a better degradation percent of methyl orange in reactions catalyzed by biotemplated catalysts (96.6%) than in commercial P25 (28%) or non-catalyzed reactions. This massive difference in the degradation percent can be attributed to the presence of carbon, which widens the absorption spectra of TiO<sub>2</sub> towards the visible region. These results suggest that C-doped TiO<sub>2</sub> catalysts can be very useful in the degradation of water pollutants under visible light irradiation [149].

As mentioned above, heterojunctions are another possibility to improve TiO<sub>2</sub> photocatalytic performance. Some P25-based TiO<sub>2</sub>@graphitic carbon heterojunctions have been prepared by biotemplating of *Staphylococcus aureus*. These catalysts were used to induce the reduction of Cr<sup>6+</sup> into Cr<sup>3+</sup> to decrease the impact of Cr<sup>6+</sup> toxicity. The reduction reaction was performed under a 500 W xenon lamp with a 420 nm filter. The results showed that the biotemplated composites exhibited photoactivity on Cr<sup>6+</sup> reduc-



tion, whereas commercial P25 did not. Also, due to the hierarchical structure of the composites, TiO<sub>2</sub>@graphitic carbon showed higher activity in Cr<sup>6+</sup> reduction under visible light (almost complete degradation after a 240 min period) [150]. Magnabosco et al. [151] produced some TiO<sub>2</sub>/SiO<sub>2</sub> catalysts that proved to be efficient in the degradation of rhodamine B with simulated solar light. The catalysts were designed using sea urchin spines. To introduce more porosity to the structure, polystyrene nanoparticles were deposited on the surface of the spine, and some TiO<sub>2</sub> and SiO<sub>2</sub> precursors were added to form the structure. [151]. Other TiO<sub>2</sub> nanoparticles with dominantly exposed {001} facets from cellulose nanocrystals with high catalytic performance in degrading rhodamine B were also developed [152]. Some nanocomposites were synthesized by loading TiO<sub>2</sub> onto reduced graphene oxide–silver nanoparticles with extended absorption spectra towards the visible region. These composites were tested under visible light degradation of rhodamine B, where photocatalytic activity was tested with suspensions of 1 g L<sup>-1</sup> catalyst in 10 mg L<sup>-1</sup> of rhodamine B solution. Results showed that with an increasing content of graphene oxide/silver nanoparticles on the composite, photodegradation increased, but only up to a point, as more than 50 μL of graphene oxide/silver nanoparticles content resulted in a gradual drop of the photocatalytic activity (reaction rate constant of  $38 \times 10^{-4} \text{ min}^{-1}$  with 50 μL content vs.  $4 \times 10^{-4} \text{ min}^{-1}$  with 500 μL). These catalysts were also tested as antimicrobial agents and showed that the composite enhanced the inactivation rate of *E. coli* under visible light radiation in comparison to TiO<sub>2</sub> (~10 colonies vs. ~70 colonies, respectively) by producing reactive oxygen species that prevented DNA replication [153]. In another study, [154] the photocatalytic activity of TiO<sub>2</sub> nanoparticles was improved by reducing the bandgap (2.41 eV) and increasing surface area and by incorporating graphene quantum dots to slow electron–hole pair recombination. Photocatalytic experiments were carried out by adding 50 mg of the photocatalyst (TiO<sub>2</sub> nanoparticles, graphene quantum dots, P25, or the composite TiO<sub>2</sub>@graphene quantum dots) into 60 mL of a rhodamine B solution that was irradiated with a xenon lamp. Results showed that the synthesized composites exhibited a better photocatalytic performance which makes them suitable for the photodegradation of pollutants (rate coefficients of 0.149–0.170 min<sup>-1</sup> for the composites and 0.126 min<sup>-1</sup> for TiO<sub>2</sub> nanoparticles) that could be attributed to an increase in the light quantum efficiency that occurs by loading TiO<sub>2</sub> on the graphene quantum dots.

Yan et al. produced TiO<sub>2</sub>/SiO<sub>2</sub> photocatalysts from three aquatic plant leaves which served as both templates and sources of silica, to degrade gentian violet. Mixed oxides such as TiO<sub>2</sub>/SiO<sub>2</sub> structures are interesting in photocatalysis because of their specific surface area and light-harvesting efficiency. The photocatalytic activity of TiO<sub>2</sub>/SiO<sub>2</sub> samples was compared to that obtained with P25 and non-templated TiO<sub>2</sub> under simulated sunlight irradiation. The results showed that the photocatalytic activity of samples prepared by biotemplating was higher than that obtained by the other photocatalysts (degradation yields of 72.0% and 61.4% of templated samples vs. 42.4% and 24.5% of P25 and TiO<sub>2</sub> particles prepared with no template, respectively), and that it depended on the type of plant [20].

Other groups have focused on developing doped heterojunctions with TiO<sub>2</sub>. N-doped CeO<sub>2</sub>–TiO<sub>2</sub> nanosheets were prepared from Chinese rose petals to eliminate dibenzothiophene, which is one of the main organic sulfides in fuels. This doped heterojunction is expected to have better photocatalytic activity due to the extension of the energy range of photoexcitation and the increase of the charge separation. Catalyst was added to a 10 ppm oil composed of dibenzothiophene and *n*-octane and the reaction was irradiated with UV light. The highest photocatalytic desulfuration activity (93.7%) was achieved when the molar ratio of Ce and Ti was 1:1. The enhanced photocatalytic activity of combined CeO<sub>2</sub>–TiO<sub>2</sub> nanosheets is considered to be of great interest in photocatalysis for the degradation of pollutants [155].

These decontamination reactions have been tested with different photocatalysts. Serra et al. [156] developed some Ni@ZnO@ZnS shells from *Spirulina plantensis* microalgae to catalyze the degradation of methylene blue (10 ppm solution). Results were compared

with Ni@ZnO–*Spirulina* structures to study the effect of the heterostructure coating in the photocatalytic activity. Ni@ZnO@ZnS–*Spirulina* exhibited a high photocatalytic activity with a methylene blue degradation efficiency of 88.9% (artificial solar light) and 86.5% (simulated solar light), three times higher than Ni@ZnO, even after being reused up to 25 times. During the photocatalytic mineralization of pollutants, hydroxyl radicals are responsible for the degradation, and Ni@ZnO@ZnS–*Spirulina* produced 30 times more hydroxyl radicals than Ni@ZnO–*Spirulina* under UV-filtered simulated sunlight, which suggests that ZnS formed a heterojunction with Ni@ZnO that improved the photocatalytic activity of the material. These catalysts were also used in the production of bioethanol from the biomass of the *Spirulina* after its saccharification and fermentation. This process showed that this reaction presented similar yields of bioethanol production to the highest ones obtained using carbohydrates feedstocks [156]. They also developed Cu@Cu<sub>2</sub>O@CuO–microalgae (*Spirulina platensis*) photocatalysts to remove tetracycline from wastewaters under visible light radiation and so reduce the potential risks of antibiotics to human health. The results showed that 98.3% and 76.5% of tetracycline was degraded at pH 8 and 6, respectively, after 80 min of irradiation. The fact that these photocatalysts exhibit such high activity at pH 6 and 8 makes them extremely useful for water decontamination as it is the usual pH range of wastewater [157].

The enhanced light absorption capability and high surface for charge transfer of butterfly wings motivated Rodriguez et al. [24] to design some ZnO coated *M. sulkowskyi* butterfly wing through biotemplating by an atomic layer deposition technique to act as photocatalysts. To test their photocatalytic activity, a reaction was carried out where ZnO coated wings were added to 10 mL of a 20 µM methylene blue solution and irradiated with a 15 W fluorescent 365 nm lamp. Wings were coated with ZnO films of different thicknesses. The 15 nm ZnO coated butterfly wing was the fastest to degrade the dye from water, being able to reduce the concentration of methylene blue by 66.4% after being irradiated with UV light for 12 h. The results of this study show that the use of biotemplating with butterfly wings allows for the production of materials with numerous applications and, specifically, with improved photocatalytic activity. The control offered by working with this template, butterfly wings, allows for the extension of possible applications of these materials. Zinc oxide has also been combined with graphene oxide to prepare a graphene oxide–zinc oxide nanocomposite to test in methyl orange decontamination reactions. Photocatalytic experiments were carried out by adding 50 mg of the catalyst to 50 mL of  $5 \times 10^{-5}$  M methyl orange solution, which was irradiated with solar light for 2 h. The stability of the photocatalysts was evaluated in three cycles reaction, showing no significant change in its activity. The degradation rate constant for the composite was higher ( $0.024 \text{ min}^{-1}$ ) than that of commercial ZnO ( $0.008 \text{ min}^{-1}$ ), due to the narrowing of the bandgap of the composite, which allows it to absorb solar light better. Also, it could be seen that the color of the solution changed completely to transparent within 120 min of reaction and it achieved a removal rate of 97% of the pollutant [158].

Juárez et al. [159] developed gold nanowires using protein lysozyme fibrils as templates with potential use as catalysts for *p*-nitrophenol reduction into *p*-aminophenol by NaBH<sub>4</sub>. Researchers chose this reaction to test catalytic activity because the borohydride reduction of *p*-nitrophenol is known to be catalyzed by noble metals. The reaction rates were 1.5–4 times larger than those obtained in previous reactions and the catalysts showed high activity even after being recovered several times. This reaction was also used to test the catalytic activity of gold nanoparticles embedded in magnolia leaves, which resulted in active and reusable catalysts due to their structure [160], and to test the activity of four types of biopolymer-capped gold nanoparticles. Poly(-glutamic acid) gold nanoparticles showed 4–6 times more activity in this chemical reaction and could also be used as an antibacterial agent as they inhibited *Salmonella enterica* and *Escherichia coli* growth more efficiently than gentamycin [161] Qin et al. used pollen grains as a template to produce TiO<sub>2</sub>/C and SiO<sub>2</sub>/C microellipsoids with immobilized Fe<sub>2</sub>O<sub>3</sub> in the pores to use in the pho-

photocatalytic degradation of X-3B dye, which was favored by the hollow and hierarchically porous structure of the biotemplated composite [162].

Calcined layered double hydroxides (CLDH) are frequently used as photocatalysts due to their high porosity and structural properties. To be tested in the degradation of water pollutants, Liu et al. designed hierarchically porous ZnAl-CLDH/FeWO<sub>4</sub> heterojunction to obtain photocatalysts with improved efficiency. Lotus pollen was used as a template. The photocatalytic activity of the catalysts was evaluated through the degradation of Congo red. The photocatalytic degradation rate of the biotemplated catalysts was higher under visible light irradiation than the obtained by the other catalysts they used in the study, mainly due to the structure of the materials [163].

A tungsten oxide–graphene oxide (WO<sub>3</sub>–GO) nanocomposite was prepared and tested in the photocatalytic degradation of methylene blue and indigo carmine [164]. Experiments were carried out by adding 15 mg of catalyst to 75 mL of 20 ppm pollutant solution at pH 7 under solar light. The photocatalytic degradation of the dyes was enhanced by the composites (percentage of degradation of 97.03% for methylene blue and 95.43% for indigo carmine, compared to 78.96% and 94.2% of pure WO<sub>3</sub>, respectively) and it was also achieved in less time than with pure WO<sub>3</sub> (180 min compared to 270 min for methylene blue; 120 min compared to 180 min for indigo carmine). These results suggest that the WO<sub>3</sub>–GO nanocomposite is a promising photocatalyst for dye degradation, as it was also stable after three cycles, only decreasing its activity from 97% to 94%. These photocatalysts also showed antibacterial properties, as they inhibited bacterial growth under irradiation at low concentrations (2.5–5 mg mL<sup>−1</sup>), and anticancer properties, as they killed 50% of a lung cancer cell line in a concentration of 139.6 μ mL<sup>−1</sup> of nanocomposite.

#### c) Electrocatalysis

Electrocatalysis involves the reduction and oxidation of compounds due to the transfer of electrons provided by an electronic current in the presence of electrocatalysts. Biotemplating has also been used to develop green and efficient electrocatalysts to catalyze different reactions. For example, Qiu et al. [165] used cotton fibers as a template and carbon source to prepare bark-structured TiC nanowires to serve as the support for Pt electrocatalysts in methanol oxidation. The bioinspired electrocatalyst (Pt/TiC NWs) showed a current density of 348.3 mA·mgPt<sup>−1</sup>, which was 4 times higher than that of the Pt/C electrocatalyst (94.1 mA·mgPt<sup>−1</sup>). Peng et al. [166] created bioinspired Fe<sub>3</sub>C@C composites from Bodhi leaves to carry out the electrochemical reduction of nitrogen to ammonia under ambient conditions with a Faraday efficiency of 9.15%, which is comparable with that of noble metal-based catalysts.

As hydrogen production via water electrolysis is of great interest in electrocatalysis, Records et al. [167] developed some Pt-Ni(OH)<sub>2</sub> nanonetworks from M13 phage to catalyze alkaline hydrogen evolution in KOH, which showed the highest mass activity (0.17–0.39 A mgPt<sup>−1</sup> vs. 0.017–0.32 A mgPt<sup>−1</sup> of non-templated catalysts).

#### d) Other reactions

The use of diesel vehicles has deteriorated the quality of air by polluting the atmosphere through soot emissions. To reduce these emissions, oxidation catalysis has been used to lower the combustion temperature of soot. Perovskite-type catalysts are of great interest due to their promising properties, La<sub>0.9</sub>K<sub>0.1</sub>CoO<sub>3</sub> in particular. Liu et al. [168] developed La<sub>0.9</sub>K<sub>0.1</sub>CoO<sub>3</sub> catalysts from pinewood, with a high porosity and surface area (total pore volume of 0.050–0.101 cm<sup>3</sup>/g and BET surface area of 84.09–147.97 m<sup>2</sup>/g depending on the treatment of wood, respectively), that reduced soot combustion temperature to 340 °C. To test the catalytic activity of the product, a catalyst: soot solution with a mass ratio of 20:1 was analyzed by a thermal gravimetric analyzer. The result of this analysis showed that the temperature at which 10% of carbon was oxidized was reduced by 59 °C, which confirmed the potential use of La<sub>0.9</sub>K<sub>0.1</sub>CoO<sub>3</sub> catalysts in reducing soot combustion emissions.

Catalytic activity was tested via allyl alcohol catalytic hydrogenation with peptide derived Pd nanocatalysts. Modifications in the amino acid content strongly influenced the

structure of the Pd nanocatalysts, resulting in a significant amount of highly disordered surface atoms. Results showed that the catalytic reaction rate might be attributed to the available surface area; since those peptides contain histidine, the peptide is better anchored so there is less space to bind to the alcohol, resulting in a slower reaction rate [169].

Linsha et al. [170] used biotemplating to develop hierarchically porous aluminosiloxane gels to immobilize the steapsin lipase enzyme for catalytic application. This enzyme is a digestive protein in the pancreatic juice that is responsible for many chemical reactions. In this work, pollen grains from *Hibiscus rosa-sinensis* were used as patterns to develop uniform spherical particles that were distributed homogeneously in the aluminosiloxane gels. The catalytic activity of the products was tested by the hydrolysis of olive oil, showing a ~3 times higher yield than the physically bonded enzyme to aerogels; the esterification of oleic acid with methanol, where the higher conversion rate was observed with the acid: alcohol molar ratio 1:6 but was completely lost after six cycles; and the transesterification reaction involved in biodiesel production, where the immobilized enzyme showed higher stability against chemical or mechanical inactivation than the free enzyme, which highlights the potential of the immobilized enzyme in microbeads in biofuel production.

Graphene has also been used to develop photocatalysts with antibacterial and antiviral properties. It has been combined with TiO<sub>2</sub> [171], which exhibited higher antibacterial activity than bare TiO<sub>2</sub> after 4 h of solar light irradiation (improved by a factor of ~6), and WO<sub>3</sub> [172], which showed a great photocatalytic performance in virus inactivation, inactivating 99.9% of viruses after 3 h of visible light irradiation. However, even though they are promising antibacterial agents, TiO<sub>2</sub>-graphene oxide composites have been tested for being cytotoxic to minuscule animals, suggesting that more studies need to be done in order to clarify the side effects of these potential photocatalytic antibacterial agents [173].

Also, Ag-TiO<sub>2</sub>/Ag/anatase-TiO<sub>2</sub> solar light-active nanocomposites were synthesized and tested on their antibacterial activity against *E. coli*. Under solar light, these composites exhibited 1.35–6.90 times more antibacterial activity than Ag/anatase-TiO<sub>2</sub> and anatase-TiO<sub>2</sub> films. Taking these results into account, and the fact that it exhibited 11 times higher durability than the other films it was compared with, this nanocomposite is a promising photocatalyst to develop biomedical materials [174].

### 2.8. Template Replication and Potential Application of the Material

The sections above highlighted applications of synthesized biotemplated materials, but this information is not available in all papers. Some of them described the synthesis method but only mentioned potential applications those materials may have. Table 1 summarizes this information.

**Table 1.** Potential application of some materials created through biotemplating distributed by template and the type of material that was produced.

Template	Type of Material Created Using These Templates	Potential Application
Bio-organisms	Zeolites and silicon-based materials	Production of photonic materials [175].
		Catalysis [176].
		Not specified [177].
	Biopolymer and polystyrene solutions	Production of super-surfaces for antimicrobial, self-cleaning, and eukaryotic cell modulation [22].
	Metal oxides	Nanobiotechnology [178].
		Not specified [179].
	Metallic structures	Targeted drug delivery, development of biosensors [180].
		Chemical sensing, building blocks for nanostructures [181].
		Nanoelectronics, cancer therapy [182].
	Ceramics	Not specified [16,23,183,184].
Not specified [185].		
Cellular components and structures	Metallic structures	Fundamental studies [186].
		Ultra-high-density data-storage [187].
		Catalysis [188–190].
		Nanoelectronics and nanodevices [11].
		Microfluidics [191].
		MRI contrast imaging [192].
		Large-scale production of chiral materials with optical properties [193].
		Biosensing, MRI [194].
		Production of nanometer-scale electronic devices [195].
		Fabrication of customized materials [13].
	Not specified [196–202].	
	Metal oxides	Sensing, cell-manipulation [203].
		Photochemistry and optoelectronics [204].
		Catalysts supports and thermal isolation [205].
		Heterogeneous catalysis molecular separation membranes [206].
Catalysis [207].		
Not specified [208–211].		
Zeolites and silicon-based	Drug delivery, hydrogen storage [190].	
Others	Not specified [212].	
Metal oxides	Gas/liquid purification or pollutant decomposition [213].	
	Solar cells, photoelectric diodes, chemical sensors [214].	
	Substrates in microelectronic applications [215].	
	Production of nanostructures for catalysis and solar energy conversion [216].	
	Purification reactions, catalysis, adsorption, energy storage [217].	
Not specified [218–220].		

Table 1. Cont.

Template	Type of Material Created Using These Templates	Potential Application
Plants, vegetable structures and products	Zeolites and silicon-based materials	Synthesis of gold nanowires with optical properties [221].
		Synthesis of adsorbents and catalysis [222].
		Fluid sensing [223].
		Catalysis [224,225].
		Catalysis and filtration [226].
	Ceramics	Not specified [227–229].
		Sensing, catalyst carriers, support for enzyme immobilization [230].
		Nitride wood ceramics preparation [18].
		Production of filters, sensors, catalysts carriers [231].
		Low density heat insulation structures, catalyst carriers [232].
		High temperature filters and catalyst support structures [233].
		Microtools, chemical reaction or catalyst support structures [234].
		Composites manufacturing [235].
		Not specified [236–240].
		Metallic structures
	Development of terahertz electromagnetic devices [242].	
	Synthesis of microstructured objects for catalysis and electrochemistry [243].	
	Photothermal antibacterial therapy, biological detoxification, targeted delivery [244].	
	Tunable terahertz antennas design [245].	
	Others	X-Ray image storage improvement [246].
Production of eco-materials for wood ceramics design [247].		
Not specified [248].		
Fabrication of novel composites materials [249].		
Eggs and egg structures	Metal oxides	Storage of radioactive isotopes [250].
		Photocatalysis [251].
		Tailored development of ceramic materials [252].
		Not specified [253].

### 2.9. Other Applications

Biotemplating has been used in many applications that are not included in any of the previously mentioned categories. For example, Dietrich et al. [254] developed wood ceramics to evaluate the conditions in which natural petrification occurs as it is an excellent method to reconstruct ancient environments. This template was also used to construct porous oxide ceramics to immobilize Sr isotopes and to act as storage [255] and to optimize the design of silicon carbide ceramics to have a better control of their macroscopic properties [256]. Also, a similar objective was pursued by other groups that focused their studies on evaluating which techniques are best to control the template preservation for the manufacture of composite materials using protein crystals [257].

In fact, developing materials with optimized properties has been one of the main objectives of researchers focusing on biotemplating. Rahman et al. [258] used tobacco mosaic virus to develop different structured surfaces to prove the importance of wickability

in dictating critical heat flux on hydrophilic surfaces. The role of wickability was demonstrated through analyzing different samples, which showed repeatable and independent results. These findings suggest that this technique could be used for optimizing material coatings. Mathew et al. [259] found that biotemplating could optimize speckle patterns for the digital image correlation method through analyzing a template pattern, which showed useful frequency spectrum properties to improve the results of this technique, while being able to adjust scaling and noise. This technique has also improved the substrate-dependent quality of the signal of surface-enhanced Raman spectroscopy, which is an interesting detection technology in different fields due to its sensing capabilities in detecting trace or single molecules. Cai et al. [260] developed some Au nanostructures from diatom frustules via biotemplating, as Au- and Ag-covered materials showed a better signal, and exhibited a great performance, with a low limit of detection and good signal reproducibility. This suggests that this technique is a potential approach towards the development of convenient hierarchical micro-nano pillar arrays with Au that could be used in applications like the detection of low concentrations of pesticides for environment monitoring.

Finally, biotemplating has been applied to evaluate the acceleration effect of hydration in calcium alumina cement in the presence of biopolymers such as alginate [261], to develop useful materials for conducting polymer devices [262], and to evaluate cysteine-free peptide adhesion onto Au particles to ease the understanding and development of different fields such as biotemplating itself, protein aggregation, and the design of nanomaterials and devices [263].

### 3. Conclusions and Future Perspectives

This review has presented a body of work that has demonstrated that biotemplating is a promising technique readily applicable to many fields to improve material properties. Since 2000, many papers have appeared in Scopus with the criteria of “biotemplating” or “bio-templating”, where materials were applied to catalysis, energy capture and storage, cancer therapy, or bone tissue engineering, among other applications, while others were only characterized to demonstrate that the natural template had been correctly mimicked. Judging by the search that was conducted and the number of publications that appeared in the mentioned database until June 2021, it seems that this technique is at its peak and might experience a broadening of the fields of application. When only considering the last 6 years, catalysis makes up 23% of the publications with biotemplating or bio-templating as keywords. Comparing that number to the one which appears in Figure 1b (corresponding to the full 2000 to June 2021 period), it seems that biotemplating is an emerging technique for the synthesis of catalysts and suggests that, in the upcoming years, there might be more research into new bioinspired catalysts that could be applied in different chemical reactions and could incorporate the benefits that nature has always brought to natural processes, while at the same time using the evolution that science has undergone in these past decades. Energy capture and storage has also received more attention (14% in the 2000–2021 range vs. 29% in the last 6 years) in order to develop shape-controlled structures and to improve current battery efficiency conducive to current energy demand (Figure 4). Also, the use of biotemplating for the development of adsorbents to reduce pollution and materials that are beneficial for medicine might become an objective for researchers in the coming years. All in all, biotemplating evolution will reflect the scientific challenges our society will face in the coming years in climate change, pollution, sustainable energy, or medicine, to cite some examples. This will also require substantial advances in theoretical, experimental, and computational simulation studies of the different roles played by the diverse natural structures, with the synergistic contribution of researchers from different fields (e.g., physics, biology, chemistry, materials science) in a multidisciplinary approach.

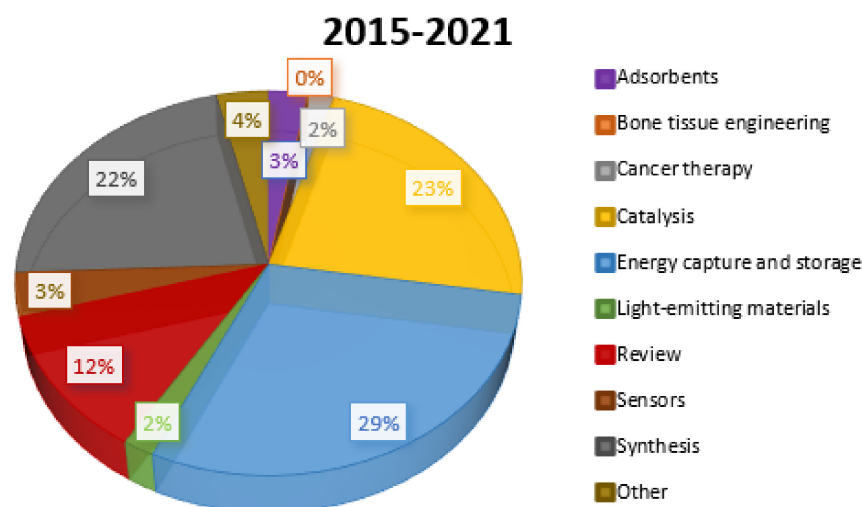


**Figure 4.** Applications of biotemplating in different fields from 2015 to June 2021. Source: Scopus, searching biotemplating or bio-templating.

**Author Contributions:** All the authors contributed equally to the search for information and writing of this work. All authors have read and agreed to the published version of the manuscript.

**Funding:** This Research was funded by MICIIN, Spain, Grant Nr: PID2019-104953RB-100; the Consejería de Transformación Económica, Industria, Conocimiento y Universidades de la Junta de Andalucía, Spain, Grant Nr. UCO-FEDER Project CATOLIVAL, Ref. 1264113-R, 2018 call; and Consejería de Transformación Económica, Industria, Conocimiento y Universidades de la Junta de Andalucía and FEDER Funds, Spain, Grant Nr. P18-RT-4822.

**Data Availability Statement:** Data sharing not applicable. No new data were created or analyzed in this study. Data sharing is not applicable to this article.

**Conflicts of Interest:** The authors declare no conflict of interest.

## References

- Hashemizadeh, I.; Tsang, D.C.W.; Ng, Y.H.; Wu, Z.; Golovko, V.; Yip, A.C.K. Bio-mimicking TiO<sub>2</sub> architectures for enhanced photocatalytic activity under UV and visible light †. *RSC Adv.* **2017**, *7*, 39098–39108. [[CrossRef](#)]
- Deshpande, A.S.; Burgert, I.; Paris, O. Natural templates. *Small* **2006**, *2*, 994–998. [[CrossRef](#)] [[PubMed](#)]
- Yang, X.Y.; Chen, L.H.; Li, Y.; Rooke, J.C.; Sanchez, C.; Su, B.L. Hierarchically porous materials: Synthesis strategies and structure design. *Chem. Soc. Rev.* **2017**, *46*, 481–558. [[CrossRef](#)] [[PubMed](#)]
- Krajina, B.A.; Proctor, A.C.; Schoen, A.P.; Spakowitz, A.J.; Heilshorn, S.C. Biotemplated synthesis of inorganic materials: An emerging paradigm for nanomaterial synthesis inspired by nature. *Prog. Mater. Sci.* **2018**, *91*, 1–23. [[CrossRef](#)]
- Deuerling, S.; Kugler, S.; Klotz, M.; Zollfrank, C.; Van Opdenbosch, D. A perspective on bio-mediated material structuring. *Adv. Mater.* **2018**, *30*, 1703656. [[CrossRef](#)] [[PubMed](#)]
- Paris, O.; Fritz-Popovski, G.; Van Opdenbosch, D.; Zollfrank, C. Recent progress in the replication of hierarchical biological tissues. *Adv. Funct. Mater.* **2013**, *23*, 4408–4422. [[CrossRef](#)]
- Paris, O.; Burgert, I.; Fratzl, P. Biomimetics and biotemplating of natural materials. *MRS Bull.* **2010**, *35*, 219–225. [[CrossRef](#)]
- Freeman, A. Protein-mediated biotemplating on the nanoscale. *Biomimetics* **2017**, *2*, 14. [[CrossRef](#)]
- Hartje, L.F.; Snow, C.D. Protein crystal based materials for nanoscale applications in medicine and biotechnology. *Wiley Interdiscip. Rev. Nanomed. Nanobiotechnology* **2019**, *11*, e1547. [[CrossRef](#)]
- Fu, Y.; Wang, X.; Zhang, J.; Li, W. Nanomaterials and nanoclusters based on DNA modulation. *Curr. Opin. Biotechnol.* **2014**, *28*, 33–38. [[CrossRef](#)]
- He, Y.; Ye, T.; Ribbe, A.E.; Mao, C. DNA-Templated Fabrication of two-dimensional metallic nanostructures by thermal evaporation coating. *J. Am. Ceram. Soc.* **2011**, *133*, 1742–1744. [[CrossRef](#)]
- Lagziel-Simis, S.; Cohen-Hadar, N.; Moscovich-Dagan, H.; Wine, Y.; Freeman, A. Protein-mediated nanoscale biotemplating. *Curr. Opin. Biotechnol.* **2006**, *17*, 569–573. [[CrossRef](#)]
- Nguyen, P.Q.; Botyanszki, Z.; Tay, P.K.R.; Joshi, N.S. Programmable biofilm-based materials from engineered curli nanofibres. *Nat. Commun.* **2014**, *5*, 4945. [[CrossRef](#)]



14. Park, J.H.; Yang, S.H.; Lee, J.; Ko, E.H.; Hong, D.; Choi, I.S. Nanocoating of single cells: From maintenance of cell viability to manipulation of cellular activities. *Adv. Mater.* **2014**, *26*, 2001–2010. [[CrossRef](#)]
15. Xia, Y.; Fang, R.; Xiao, Z.; Huang, H.; Gan, Y.; Yan, R.; Lu, X.; Liang, C.; Zhang, J.; Tao, X.; et al. Confining sulfur in N-doped porous carbon microspheres derived from microalgae for advanced lithium-sulfur batteries. *ACS Appl. Mater. Interfaces* **2017**, *9*, 23782–23791. [[CrossRef](#)]
16. Adigun, O.O.; Novikova, G.; Retzlaff-Roberts, E.L.; Kim, B.S.; Miller, J.T.; Loesch-Fries, L.S.; Harris, M.T. Decoupling and elucidation of surface-driven processes during inorganic mineralization on virus templates. *J. Colloid Interface Sci.* **2016**, *483*, 165–176. [[CrossRef](#)]
17. Li, L.; Belcher, A.M.; Loke, D.K. Simulating selective binding of a biological template to a nanoscale architecture: A core concept of a clamp-based binding-pocket-favored N-terminal-domain assembly. *Nanoscale* **2020**, *12*, 24214–24227. [[CrossRef](#)]
18. Luo, M.; Gao, J.; Zhang, X.; Yang, J.; Hou, G.; Ouyang, D.; Jin, Z. Processing of porous TiN/C ceramics from biological templates. *Mater. Lett.* **2007**, *61*, 186–188. [[CrossRef](#)]
19. Kang, Y.S.; Kim, D.Y.; Yoon, J.; Park, J.W.; Kim, G.; Ham, Y.; Park, I.; Koh, M.; Park, K. Shape control of hierarchical lithium cobalt oxide using biotemplates for connected nanoparticles. *J. Power Sources* **2019**, *436*, 226836. [[CrossRef](#)]
20. Yan, Z.; He, J.; Guo, L.; Li, Y.; Duan, D.; Chen, Y.; Li, J.; Yuan, F.; Wang, J. Biotemplated mesoporous TiO<sub>2</sub>/SiO<sub>2</sub> composite derived from aquatic plant leaves for efficient dye degradation. *Catalysts* **2017**, *7*, 82. [[CrossRef](#)]
21. Hidalgo-Carrillo, J.; Martín-Gómez, J.; Herrera-Beurnio, M.C.; Estévez, R.C.; Urbano, F.J.; Marinas, A. Olive leaves as biotemplates for enhanced solar-light harvesting by a titania-based solid. *Nanomaterials* **2020**, *10*, 1057. [[CrossRef](#)]
22. Green, D.W.; Lee, K.K.H.; Watson, J.A.; Kim, H.Y.; Yoon, K.S.; Kim, E.J.; Lee, J.M.; Watson, G.S.; Jung, H.S. High quality bioreplication of intricate nanostructures from a fragile gecko skin surface with bactericidal properties. *Sci. Rep.* **2017**, *7*, 41023. [[CrossRef](#)]
23. He, Z.; Zhang, W.; Wang, W.; Tassin, M.; Gu, J.; Liu, Q.; Zhu, S.; Su, H.; Feng, C.; Zhang, D. Fabrication of Fe-wings used for micro imprinting with a natural butterfly wing structure by in situ carbothermic reduction. *J. Mater. Chem. B* **2013**, *1*, 1673–1677. [[CrossRef](#)]
24. Rodríguez, R.E.; Agarwal, S.P.; An, S.; Kazyak, E.; Das, D.; Shang, W.; Skye, R.; Deng, T.; Dasgupta, N.P. Biotemplated morpho butterfly wings for tunable structurally colored photocatalysts. *ACS Appl. Mater. Interfaces* **2018**, *10*, 4614–4621. [[CrossRef](#)]
25. Tong, X.; Zhou, D.; Qiu, M.; Zhou, Y.; Ai, Y.; Guo, X.; Zhang, J.; Cai, Y.; Kong, Q. Biomimetic NiO/Ni with a regular pore-array structure as a supercapacitor electrode material. *Eur. J. Inorg. Chem.* **2021**, *2021*, 562–566. [[CrossRef](#)]
26. Van Opdenbosch, D.; Johannes, M.; Wu, X.; Fabritius, H.; Zollfrank, C. Fabrication of three-dimensional photonic crystals with tunable photonic properties by biotemplating. *Photonics Nanostructures-Fundam. Appl.* **2012**, *10*, 516–522. [[CrossRef](#)]
27. Kamata, K.; Piao, Z.; IyodaTokyo, T. Biotemplating process for 3D structured materials. *Int. Polym. Sci. Technol.* **2014**, *87*, 140–145. [[CrossRef](#)]
28. Zhou, H.; Fan, T.; Zhang, D. Biotemplated materials for sustainable energy and environment: Current status and challenges. *ChemSusChem* **2011**, *4*, 1344–1387. [[CrossRef](#)]
29. Chao, J.T.; Biggs, M.J.P.; Pandit, A.S. Diatoms: A biotemplating approach to fabricating drug delivery reservoirs. *Expert Opin. Drug Deliv.* **2014**, *11*, 1687–1695. [[CrossRef](#)] [[PubMed](#)]
30. Zollfrank, C. Biotemplating: Polysaccharides in materials engineering. *WIT Trans. Ecol. Environ.* **2010**, *138*, 441–451. [[CrossRef](#)]
31. Zollfrank, C.; Cromme, P.; Rauch, M.; Scheel, H.; Kostova, M.H.; Gutbrod, K.; Gruber, S.; van Opdenbosch, D. Biotemplating of inorganic functional materials from polysaccharides. *Bioinspired Biomim. Nanobiomaterials* **2012**, *1*, 13–25. [[CrossRef](#)]
32. Boury, B.; Plumejeau, S. Metal oxides and polysaccharides: An efficient hybrid association for materials chemistry. *Green Chem.* **2015**, *17*, 72–88. [[CrossRef](#)]
33. Behrens, S.S. Synthesis of inorganic nanomaterials mediated by protein assemblies. *J. Mater. Chem.* **2008**, *18*, 3788–3798. [[CrossRef](#)]
34. Tao, K.; Levin, A.; Adler-Abramovich, L.; Gazit, E. Fmoc-modified amino acids and short peptides: Simple bio-inspired building blocks for the fabrication of functional materials. *Chem. Soc. Rev.* **2016**, *45*, 3935–3953. [[CrossRef](#)]
35. Butt, H.; Yetisen, A.K.; Mistry, D.; Khan, S.A.; Hassan, M.U.; Yun, S.H. Morpho butterfly-inspired nanostructures. *Adv. Opt. Mater.* **2016**, *4*, 497–504. [[CrossRef](#)]
36. Sotiropoulou, S.; Sierra-Sastre, Y.; Mark, S.S.; Batt, C.A. Biotemplated nanostructured materials. *Chem. Mater.* **2008**, *20*, 821–834. [[CrossRef](#)]
37. Zelechowska, K. Methods of ZnO nanoparticles synthesis. *BioTechnologia* **2014**, *95*, 150–159. [[CrossRef](#)]
38. Plumejeau, S.; Alauzun, J.G.; Boury, B. Hybrid metal oxide@biopolymer materials precursors of metal oxides and metal oxide-carbon composites. *J. Ceram. Soc. Jpn.* **2015**, *123*, 695–708. [[CrossRef](#)]
39. Van Opdenbosch, D.; Fritz-Popovski, G.; Plank, J.; Zollfrank, C.; Paris, O. Passive and active mechanical properties of biotemplated ceramics revisited. *Bioinspiration Biomim.* **2016**, *11*, 065001. [[CrossRef](#)]
40. Davis, S.A.; Dujardin, E.; Mann, S. Biomolecular inorganic materials chemistry. *Curr. Opin. Solid State Mater. Sci.* **2003**, *7*, 273–281. [[CrossRef](#)]
41. Müller, C.; Ouyang, L.; Lund, A.; Moth-Poulsen, K.; Hamedi, M.M. From single molecules to thin film electronics, nanofibers, e-textiles and power cables: Bridging length scales with organic semiconductors. *Adv. Mater.* **2019**, *31*, 1807286. [[CrossRef](#)] [[PubMed](#)]

42. Wu, L.; He, J.; Shang, W.; Deng, T.; Gu, J.; Su, H.; Liu, Q.; Zhang, W.; Zhang, D. Optical functional materials inspired by biology. *Adv. Opt. Mater.* **2016**, *4*, 195–224. [[CrossRef](#)]
43. Jorgensen, M.R.; Bartl, M.H. Biotemplating routes to three-dimensional photonic crystals. *J. Mater. Chem.* **2011**, *21*, 10583–10591. [[CrossRef](#)]
44. Tan, K.B.; Sun, D.; Huang, J.; Odoom-Wubah, T.; Li, Q. State of arts on the bio-synthesis of noble metal nanoparticles and their biological application. *Chinese J. Chem. Eng.* **2021**, *30*, 272–290. [[CrossRef](#)]
45. Ghani, M. Nanocrystalline cellulose as a biotemplate for preparation of porous titania thin film as a sorbent for thin film microextraction of ketorolac, meloxicam, diclofenac and mefenamic acid. *J. Chromatogr. B* **2020**, *1142*, 122039. [[CrossRef](#)]
46. Wang, W.; Chen, B.; Huang, Y. Eggshell membrane-based biotemplating of mixed hemimicelle/admicelle as a solid-phase extraction adsorbent for carcinogenic polycyclic aromatic hydrocarbons. *J. Agric. Food Chem.* **2014**, *62*, 8051–8059. [[CrossRef](#)]
47. Zwir-Ferenc, A.; Biziuk, M. Solid phase extraction technique—Trends, opportunities and applications. *Polish J. Environ. Stud.* **2006**, *15*, 677–690.
48. Sun, Q.; Chen, B. Biotemplated fabrication of 3D hierarchically Porous MgAl-LDH/CF composites with effective adsorption of organic dyes from wastewater. *Ind. Eng. Chem. Res.* **2020**, *59*, 16838–16850. [[CrossRef](#)]
49. Inbaraj, B.S.; Sridhar, K.; Chen, B.-H. Removal of polycyclic aromatic hydrocarbons from water by magnetic activated carbon nanocomposite from green tea waste. *J. Hazard. Mater.* **2021**, *415*, 125701. [[CrossRef](#)]
50. Suvindran, N.; Li, F.; Pan, Y.; Zhao, X. Characterization and bioreplication of *tridactantia pallida* inspired biomimetic superwettability for dual way patterned water harvesting. *Adv. Mater. Interfaces* **2018**, *5*, 1800723. [[CrossRef](#)]
51. Akhavan, O.; Ghaderi, E. Graphene nanomesh promises extremely efficient in vivo photothermal therapy. *Small* **2013**, *9*, 3593–3601. [[CrossRef](#)]
52. Jiang, W.; Mo, F.; Jin, X.; Chen, L.; Xu, L.; Guo, L.; Fu, F. Tumor-targeting photothermal heating-responsive nanoplatform based on reduced graphene oxide/mesoporous silica/hyaluronic acid nanocomposite for enhanced photodynamic therapy. *Adv. Mater. Interfaces* **2017**, *4*, 1700425. [[CrossRef](#)]
53. Lima-Sousa, R.; de Melo-Diogo, D.; Alves, C.G.; Costa, E.C.; Ferreira, P.; Louro, R.O.; Correia, I.J. Hyaluronic acid functionalized green reduced graphene oxide for targeted cancer photothermal therapy. *Carbohydr. Polym.* **2018**, *200*, 93–99. [[CrossRef](#)]
54. Abdolahad, M.; Janmaleki, M.; Mohajezadeh, S.; Akhavan, O.; Abbasi, S. Polyphenols attached graphene nanosheets for high efficiency NIR mediated photodestruction of cancer cells. *Mater. Sci. Eng. C* **2013**, *33*, 1498–1505. [[CrossRef](#)]
55. Akhavan, O.; Ghaderi, E.; Aghayee, S.; Fereydooni, Y.; Talebi, A. The use of a glucose-reduced graphene oxide suspension for photothermal cancer therapy. *J. Mater. Chem.* **2012**, *22*, 13773–13781. [[CrossRef](#)]
56. Xue, W.; Zhou, J.; Gao, D.; Gao, F.; Wang, Z.; Luo, L.; Li, Y.; Liu, Z. Preparation of adenovirus-templated gold nanoshells and a study of their photothermal therapy efficacy. *New J. Chem.* **2015**, *39*, 3608–3614. [[CrossRef](#)]
57. Shukla, S.; Eber, F.J.; Nagarajan, A.S.; DiFranco, N.A.; Schmidt, N.; Wen, A.M.; Eiben, S.; Twyman, R.M.; Wege, C.; Steinmetz, N.F. The impact of aspect ratio on the biodistribution and tumor homing of rigid soft-matter nanorods. *Adv. Healthc. Mater.* **2015**, *4*, 874–882. [[CrossRef](#)]
58. Akhavan, O.; Ghaderi, E.; Emamy, H. Nontoxic concentrations of PEGylated graphene nanoribbons for selective cancer cell imaging and photothermal therapy. *J. Mater. Chem.* **2012**, *22*, 20626–20633. [[CrossRef](#)]
59. Omid, S.; Pirhayati, M.; Kakanejadifard, A. Co-delivery of doxorubicin and urcumin by a pH-sensitive, injectable, and in situ hydrogel composed of chitosan, graphene, and cellulose nanowhisker. *Carbohydr. Polym.* **2020**, *231*, 115745. [[CrossRef](#)]
60. Ayazi, H.; Akhavan, O.; Raoufi, M.; Varshochian, R.; Hosseini Motlagh, N.S.; Atyabi, F. Graphene aerogel nanoparticles for in-situ loading/pH sensitive releasing anticancer drugs. *Colloids Surfaces B Biointerfaces* **2020**, *186*, 110712. [[CrossRef](#)]
61. Qian, J.; Yong, X.; Xu, W.; Jin, X. Preparation and characterization of bimodal porous poly( $\gamma$ -benzyl-L- glutamate) scaffolds for bone tissue engineering. *Mater. Sci. Eng. C* **2013**, *33*, 4587–4593. [[CrossRef](#)]
62. Qian, J.; Kang, Y.; Zhang, W.; Li, Z. Fabrication, chemical composition change and phase evolution of biomorphic hydroxyapatite. *J. Mater. Sci. Mater. Med.* **2008**, *19*, 3373–3383. [[CrossRef](#)]
63. Qian, J.; Kang, Y.; Wei, Z.; Zhang, W. Fabrication and characterization of biomorphic 45S5 bioglass scaffold from sugarcane. *Mater. Sci. Eng. C* **2009**, *29*, 1361–1364. [[CrossRef](#)]
64. Kim, M.K.; Kim, J.J.; Shin, U.S.; Kim, H.W. Production of a biomimetic apatite nanotube mesh via biotemplating a polymer nanofiber mesh. *Mater. Lett.* **2010**, *64*, 2655–2658. [[CrossRef](#)]
65. Ramay, H.R.R.; Zhang, M. Biphasic calcium phosphate nanocomposite porous scaffolds for load-bearing bone tissue engineering. *Biomaterials* **2004**, *25*, 5171–5180. [[CrossRef](#)]
66. Fabbri, P.; Bondioli, F.; Messori, M.; Bartoli, C.; Dinucci, D.; Chiellini, F. Porous scaffolds of polycaprolactone reinforced with in situ generated hydroxyapatite for bone tissue engineering. *J. Mater. Sci. Mater. Med.* **2010**, *21*, 343–351. [[CrossRef](#)]
67. Qian, J.; Xu, M.; Suo, A.; Yang, T.; Yong, X. An innovative method to fabricate honeycomb-like poly( $\epsilon$ -caprolactone)/nano-hydroxyapatite scaffolds. *Mater. Lett.* **2013**, *93*, 72–76. [[CrossRef](#)]
68. Qian, J.; Suo, A.; Jin, X.; Xu, W.; Xu, M. Preparation and in vitro characterization of biomorphic silk fibroin scaffolds for bone tissue engineering. *J. Biomed. Mater. Res.-Part A* **2014**, *102*, 2961–2971. [[CrossRef](#)] [[PubMed](#)]
69. Popat, K.C.; Daniels, R.H.; Dubrow, R.S.; Hardev, V.; Desai, T.A. Nanostructured surfaces for bone biotemplating applications. *J. Orthop. Res.* **2006**, *24*, 619–627. [[CrossRef](#)]

70. Akhavan, O.; Ghaderi, E.; Shahsavari, M. Graphene nanogrids for selective and fast osteogenic differentiation of human mesenchymal stem cells. *Carbon* **2013**, *59*, 200–211. [[CrossRef](#)]
71. Rahighi, R.; Panahi, M.; Akhavan, O.; Mansoorianfar, M. Pressure-engineered electrophoretic deposition for gentamicin loading within osteoblast-specific cellulose nanofiber scaffolds. *Mater. Chem. Phys.* **2021**, *272*, 125018. [[CrossRef](#)]
72. Akhavan, O.; Ghaderi, E.; Shirazian, S.A.; Rahighi, R. Rolled graphene oxide foams as three-dimensional scaffolds for growth of neural fibers using electrical stimulation of stem cells. *Carbon* **2016**, *97*, 71–77. [[CrossRef](#)]
73. Akhavan, O.; Ghaderi, E.; Abouei, E.; Hatamie, S.; Ghasemi, E. Accelerated differentiation of neural stem cells into neurons on ginseng-reduced graphene oxide sheets. *Carbon* **2014**, *66*, 395–406. [[CrossRef](#)]
74. Wang, Y.; Lee, W.C.; Manga, K.K.; Ang, P.K.; Lu, J.; Liu, Y.P.; Lim, C.T.; Loh, K.P. Fluorinated graphene for promoting neuro-induction of stem cells. *Adv. Mater.* **2012**, *24*, 4285–4290. [[CrossRef](#)]
75. Akhavan, O.; Ghaderi, E. Differentiation of human neural stem cells into neural networks on graphene nanogrids. *J. Mater. Chem. B* **2013**, *1*, 6291–6301. [[CrossRef](#)]
76. Alipour, A.; Gholami, A. Virus Decorated Nanobiomaterials as Scaffolds for Tissue Engineering. *Adv. Appl. NanoBio-Technol.* **2021**, *2*, 79–85.
77. Zhang, Y.; Dong, Y.; Zhou, J.; Li, X.; Wang, F. Application of plant viruses as a biotemplate for nanomaterial fabrication. *Molecules* **2018**, *23*, 2311. [[CrossRef](#)]
78. Young, M.; Willits, D.; Uchida, M.; Douglas, T. Plant viruses as biotemplates for materials and their use in nanotechnology. *Annu. Rev. Phytopathol.* **2008**, *46*, 361–384. [[CrossRef](#)]
79. Yu, Y.; Zheng, X.T.; Yee, B.W.; Tan, Y.N. Biomimicking synthesis of photoluminescent molecular lantern catalyzed by in-situ formation of nanogold catalysts. *Mater. Sci. Eng. C* **2017**, *77*, 1111–1116. [[CrossRef](#)]
80. Rambo, C.R.; Hotza, D.; da Cunha, C.R.; Zollfrank, C. Directed photoluminescent emission of ZnO tetrapods on biotemplated Al<sub>2</sub>O<sub>3</sub>. *Opt. Mater.* **2013**, *36*, 562–567. [[CrossRef](#)]
81. Santos, S.C.; Yamagata, C.; Silva, A.C.; Setz, L.F.G.; Mello-Castanho, S.R.H. Yttrium disilicate micro-cellular architecture from biotemplating of luffa cylindrica. *J. Ceram. Sci. Technol.* **2014**, *5*, 203–208. [[CrossRef](#)]
82. Santos, S.C.; Yamagata, C.; Campos, L.L.; Mello-Castanho, S.R.H. Processing and thermoluminescent response of porous biomorphic dysprosium doped yttrium disilicate burner. *Mater. Chem. Phys.* **2016**, *177*, 505–511. [[CrossRef](#)]
83. Ivanova, A.; Frka-Petecic, B.; Paul, A.; Wagner, T.; Jumabekov, A.N.; Vilk, Y.; Weber, J.; Schmedt Auf Der Günne, J.; Vignolini, S.; Tiemann, M.; et al. Cellulose nanocrystal-templated tin dioxide thin films for gas sensing. *ACS Appl. Mater. Interfaces* **2020**, *12*, 12639–12647. [[CrossRef](#)]
84. Zhu, Y.; Su, H.; Chen, Y.; Jin, Z.; Xu, J.; Zhang, D. A facile synthesis of PdO-decorated SnO<sub>2</sub> nanocomposites with open porous hierarchical architectures for gas sensors. *J. Am. Ceram. Soc.* **2016**, *99*, 3770–3774. [[CrossRef](#)]
85. Yu, S.; Li, L.; Wang, J.; Liu, E.; Zhao, J.; Xu, F.; Cao, Y.; Lu, C. Light-boosting highly sensitive pressure sensors based on bioinspired multiscale surface structures. *Adv. Funct. Mater.* **2020**, *30*, 1907091. [[CrossRef](#)]
86. Shi, J.; Lv, S.; Wang, L.; Dai, Z.; Yang, S.; Zhao, L.; Tian, H.; Du, M.; Li, H.; Fang, Y. Crack Control in Biotemplated Gold Films for Wide-Range, Highly Sensitive Strain Sensing. *Adv. Mater. Interfaces* **2019**, *6*, 1901223. [[CrossRef](#)]
87. Kostovski, G.; White, D.J.; Mitchell, A.; Austin, M.W.; Stoddart, P.R. Nanoimprinted optical fibres: Biotemplated nanostructures for SERS sensing. *Biosens. Bioelectron.* **2008**, *24*, 1531–1535. [[CrossRef](#)]
88. Akhavan, O.; Ghaderi, E.; Rahighi, R. Toward Single-DNA electrochemical biosensing by graphene nanowalls. *ACS Nano* **2012**, *6*, 2904–2916. [[CrossRef](#)]
89. Akhavan, O.; Ghaderi, E.; Hashemi, E.; Rahighi, R. Ultra sensitive detection of leukemia by graphene. *Nanoscale* **2014**, *6*, 14810–14819. [[CrossRef](#)]
90. Akhavan, O.; Ghaderi, E.; Rahighi, R.; Abdollahad, M. Spongy graphene electrode in electrochemical detection of leukemia at single-cell levels. *Carbon* **2014**, *79*, 654–663. [[CrossRef](#)]
91. Akhavan, O.; Ghaderi, E. Copper oxide nanoflakes as highly sensitive and fast response self-sterilizing biosensors. *J. Mater. Chem.* **2011**, *21*, 12935–12940. [[CrossRef](#)]
92. Akhavan, O.; Ghaderi, E. Escherichia coli bacteria reduce graphene oxide to bactericidal graphene in a self-limiting manner. *Carbon* **2011**, *50*, 1853–1860. [[CrossRef](#)]
93. Xue, G.; Yu, W.; Yutong, L.; Qiang, Z.; Xiuying, L.; Yiwei, T.; Jianrong, L. Construction of novel xanthine biosensor by using Zinc Oxide (ZnO) by biotemplate method for fish freshness detection. *Anal. Methods* **2019**, *11*, 1021–1026. [[CrossRef](#)]
94. Barannikova, E.A.; Riley, S.J.; Allen, M.A. Bioprospecting solid binding polypeptides for lithium ion battery cathode materials. *Biointerphases* **2019**, *14*, 051007–1–8. [[CrossRef](#)]
95. Jeong, C.K.; Kim, I.; Park, K.I.; Oh, M.H.; Paik, H.; Hwang, G.T.; No, K.; Nam, Y.S.; Lee, K.J. Virus-directed design of a flexible BaTiO<sub>3</sub> nanogenerator. *ACS Nano* **2013**, *7*, 11016–11025. [[CrossRef](#)]
96. Gan, Y.; Xu, F.; Luo, J.; Yuan, H.; Jin, C.; Zhang, L.; Fang, C.; Sheng, O.; Huang, H.; Xia, Y.; et al. One-pot biotemplate synthesis of FeS<sub>2</sub> decorated sulfur-doped carbon fiber as high capacity anode for lithium-ion batteries. *Electrochim. Acta* **2016**, *209*, 201–209. [[CrossRef](#)]
97. Mirvaux, B.; Recham, N.; Miot, J.; Courty, M.; Bernard, S.; Beyssac, O.; Davoisne, C.; Sougrati, M.; Demortiere, A.; Guyot, F.; et al. Iron phosphate/bacteria composites as precursors for textured electrode materials with enhanced electrochemical properties. *J. Electrochemical Soc.* **2016**, *163*, A2139–A2148. [[CrossRef](#)]

98. Dylla, A.G.; Henkelman, G.; Stevenson, K.J. Lithium insertion in nanostructured TiO<sub>2</sub> (B) architectures. *Acc. Chem. Res.* **2013**, *46*, 1104–1112. [[CrossRef](#)]
99. Henry, A.; Plumejeau, S.; Heux, L.; Louvain, N.; Monconduit, L.; Stievano, L.; Boury, B. Conversion of nanocellulose aerogel into TiO<sub>2</sub> and TiO<sub>2</sub>@C nano-thorns by direct anhydrous mineralization with TiCl<sub>4</sub>. Evaluation of electrochemical properties in Li batteries. *ACS Appl. Mater. Interfaces* **2015**, *7*, 14584–14592. [[CrossRef](#)]
100. Kim, S.W.; Han, T.H.; Kim, J.; Gwon, H.; Moon, H.S.; Kang, S.W.; Kim, S.O.; Kang, K. Fabrication and electrochemical characterization of TiO<sub>2</sub> three-dimensional nanonetwork based on peptide assembly. *ACS Nano* **2009**, *3*, 1085–1090. [[CrossRef](#)]
101. Li, B.; Zai, J.; Xiao, Y.; Han, Q.; Qian, X. SnO<sub>2</sub>/C composites fabricated by a biotemplating method from cotton and their electrochemical performances. *CrystEngComm* **2014**, *16*, 3318–3322. [[CrossRef](#)]
102. Ping, H.; Poudel, L.; Xie, H.; Fang, W.; Zou, Z.; Zhai, P.; Wagermaier, W.; Fratzl, P.; Wang, W.; Wang, H.; et al. Synthesis of monodisperse rod-shaped silica particles through biotemplating of surface-functionalized bacteria. *Nanoscale* **2020**, *12*, 8732–8741. [[CrossRef](#)]
103. Xia, Y.; Zhang, W.; Xiao, Z.; Huang, H.; Zeng, H.; Chen, X.; Chen, F.; Gan, Y.; Tao, X. Biotemplated fabrication of hierarchically porous NiO/C composite from lotus pollen grains for lithium-ion batteries. *J. Mater. Chem.* **2012**, *22*, 9209–9215. [[CrossRef](#)]
104. Wang, J.; Liu, W.; Liu, S.; Chen, J.; Wang, H.; Zhao, S. Biomass derived fabrication of a novel sea cucumber-like LiMn<sub>2</sub>O<sub>4</sub>/C composite with a hierarchical porous structure as the cathode for lithium-ion batteries. *Electrochim. Acta* **2016**, *188*, 645–652. [[CrossRef](#)]
105. Wang, J.; Liu, W.; Chen, J.; Wang, H.; Liu, S.; Chen, S. Biotemplated MnO/C microtubes from spirogyra with improved electrochemical performance for lithium-ion batteries. *Electrochim. Acta* **2016**, *188*, 210–217. [[CrossRef](#)]
106. Xia, Y.; Xiao, Z.; Dou, X.; Huang, H.; Lu, X.; Yan, R.; Gan, Y.; Zhu, W.; Tu, J.; Zhang, W.; et al. Green and facile fabrication of hollow porous MnO/C microspheres from microalgae for lithium-ion batteries. *ACS Nano* **2013**, *7*, 7083–7092. [[CrossRef](#)]
107. Xia, Y.; Zhang, W.; Huang, H.; Gan, Y.; Xiao, Z.; Qian, L.; Tao, X. Biotemplating of phosphate hierarchical rechargeable LiFePO<sub>4</sub>/C spirulina microstructures. *J. Mater. Chem.* **2011**, *21*, 6498–6501. [[CrossRef](#)]
108. Yan, D.; Luo, X.; Zhang, H.; Zhu, G.; Chen, L.; Chen, G.; Xu, H.; Yu, A. Single-crystalline a-MoO<sub>3</sub> microbelts derived from a bio-templating method for superior lithium storage application. *J. Alloys Compd.* **2016**, *688*, 481–486. [[CrossRef](#)]
109. Zhu, W.; Huang, H.; Zhang, W.; Tao, X.; Gan, Y.; Xia, Y.; Yang, H.; Guo, X. Synthesis of MnO/C composites derived from pollen template for advanced lithium-ion batteries. *Electrochim. Acta* **2015**, *152*, 286–293. [[CrossRef](#)]
110. Xia, Y.; Fang, R.; Xiao, Z.; Ruan, L.; Yan, R.; Huang, H.; Liang, C.; Gan, Y.; Zhang, J.; Tao, X.; et al. Supercritical fluid assisted biotemplating synthesis of Si-O-C microspheres from microalgae for advanced Li-ion batteries. *RSC Adv.* **2016**, *6*, 69764–69772. [[CrossRef](#)]
111. Xia, Y.; Zhong, H.; Fang, R.; Liang, C.; Xiao, Z.; Huang, H.; Gan, Y.; Zhang, J.; Tao, X.; Zhang, W. Biomass derived Ni(OH)<sub>2</sub>@porous carbon/sulfur composites synthesized by a novel sulfur impregnation strategy based on supercritical CO<sub>2</sub> technology for advanced Li-S batteries. *J. Power Sources* **2018**, *378*, 73–80. [[CrossRef](#)]
112. Fang, R.; Xia, Y.; Liang, C.; He, X.; Huang, H.; Gan, Y.; Zhang, J.; Tao, X.; Zhang, W. Supercritical CO<sub>2</sub>-assisted synthesis of 3D porous SiOC/Se cathode for ultrahigh areal capacity and long cycle life Li–Se batteries. *J. Mater. Chem. A* **2018**, *6*, 24773–24782. [[CrossRef](#)]
113. Dong, B.; Driscoll, L.L.; Stockham, M.P.; Kendrick, E.; Slater, P.R. Low temperature synthesis of garnet solid state electrolytes: Implications on aluminium incorporation in Li<sub>7</sub>La<sub>3</sub>Zr<sub>2</sub>O<sub>12</sub>. *Solid State Ionics* **2020**, *350*, 115317. [[CrossRef](#)]
114. Kong, Y.; Luo, J.; Jin, C.; Yuan, H.; Sheng, O.; Zhang, L.; Fang, C.; Zhang, W.; Huang, H.; Xia, Y.; et al. Enhanced sulfide chemisorption by conductive Al-doped ZnO decorated carbon nanoflakes for advanced Li–S. *Nano Res.* **2018**, *11*, 477–489. [[CrossRef](#)]
115. Tao, X.; Wang, J.; Liu, C.; Wang, H.; Yao, H.; Zheng, G.; Seh, Z.W.; Cai, Q.; Li, W.; Zhou, G.; et al. Balancing surface adsorption and diffusion of lithium-polysulfides on nonconductive oxides for lithium–sulfur battery design. *Nat. Commun.* **2016**, *7*, 11203. [[CrossRef](#)]
116. Tao, X.; Wu, R.; Xia, Y.; Huang, H.; Chai, W.; Feng, T.; Gan, Y.; Zhang, W. Biotemplated fabrication of Sn@C anode materials based on the unique metal biosorption behavior of microalgae. *ACS Appl. Mater. Interfaces* **2014**, *6*, 3696–3702. [[CrossRef](#)]
117. Hu, J.; Yuan, X.; Wang, C.; Shao, X.; Yang, B.; Razaq, A.A.; Zhao, X.; Lian, Y.; Deng, Z.; Chen, M.; et al. Self-phosphorization of MOF-armored microbes for advanced energy storage. *Small* **2020**, *16*, 2000755. [[CrossRef](#)]
118. Oh, D.; Ozgit-Akgun, C.; Akca, E.; Thompson, L.E.; Tadesse, L.F.; Kim, H.C.; Demirci, G.; Miller, R.D.; Maune, H. Biotemplating pores with size and shape diversity for Li-oxygen battery cathodes. *Sci. Rep.* **2017**, *7*, 45919. [[CrossRef](#)]
119. Atalay, F.E.; Asma, D.; Kaya, H.; Ozbey, E. The fabrication of metal oxide nanostructures using *Deinococcus radiodurans* bacteria for supercapacitor. *Mater. Sci. Semicond. Process.* **2015**, *38*, 314–318. [[CrossRef](#)]
120. Gong, L.; Liu, X.; Su, L.; Wang, L. Synthesis and electrochemical capacitive behaviors of Co<sub>3</sub>O<sub>4</sub> nanostructures from a novel biotemplating technique. *J. Solid State Electrochem.* **2012**, *16*, 297–304. [[CrossRef](#)]
121. Kong, L.; Zhang, C.; Wang, J.; Long, D.; Qiao, W.; Ling, L. Ultrahigh intercalation pseudocapacitance of mesoporous orthorhombic niobium pentoxide from a novel cellulose nanocrystal template. *Mater. Chem. Phys.* **2015**, *149–150*, 495–504. [[CrossRef](#)]
122. Hao, J.; Huang, Y.; He, C.; Xu, W.; Yuan, L.; Shu, D.; Song, X.; Meng, T. Bio-templated fabrication of three-dimensional network activated carbons derived from mycelium pellets for supercapacitor applications. *Sci. Rep.* **2018**, *8*, 562. [[CrossRef](#)]

123. Chang, C.M.; Hu, Z.H.; Lee, T.Y.; Huang, Y.A.; Ji, W.F.; Liu, W.R.; Yeh, J.M.; Wei, Y. Biotemplated hierarchical polyaniline composite electrodes with high performance for flexible supercapacitors. *J. Mater. Chem. A* **2016**, *4*, 9133–9145. [[CrossRef](#)]
124. Gerasopoulos, K.; Pomerantseva, E.; McCarthy, M.; Brown, A.; Wang, C.; Culver, J.; Ghodssi, R. Hierarchical three-dimensional microbattery electrodes combining bottom-up self-assembly and top-down micromachining. *ACS Nano* **2012**, *6*, 6422–6432. [[CrossRef](#)]
125. Records, W.C.; Wei, S.; Belcher, A.M. Virus-templated nickel phosphide nanofoams as additive-free, thin-film Li-ion microbattery anodes. *Small* **2019**, *15*, 1903166. [[CrossRef](#)]
126. Xue, W.; Li, Y.; Zhou, J.; Wang, Z.; Liu, Y.; Zhang, X.; Liu, Z.; Gao, F.; Gao, D. Self-assembly of adenovirus-templated platinum nanoshells and evaluation of their biocompatibilities. *RSC Adv.* **2015**, *5*, 86381–86386. [[CrossRef](#)]
127. Gao, Z.D.; Liu, H.F.; Song, Y.Y. Biotemplated synthesis of Au nanoparticles-TiO<sub>2</sub> nanotube junctions for enhanced direct electrochemistry of heme proteins. *Chem. Commun.* **2013**, *49*, 774–776. [[CrossRef](#)]
128. Brotto, J.O.; Padoin, N.; Rambo, C.R.; Soares, C. Biomorphic microchanneled electrodes for enhanced water desalination through capacitive deionization. *Water Supply* **2019**, *19*, 1221–1228. [[CrossRef](#)]
129. Dorval Courchesne, N.M.; Klug, M.T.; Huang, K.J.; Weidman, M.C.; Cantú, V.J.; Chen, P.Y.; Kooi, S.E.; Yun, D.S.; Tisdale, W.A.; Fang, N.X.; et al. Constructing multifunctional virus-templated nanoporous composites for thin film solar cells: Contributions of morphology and optics to photocurrent generation. *J. Phys. Chem.* **2015**, *119*, 13987–14000. [[CrossRef](#)]
130. Han, T.H.; Moon, H.S.; Hwang, J.O.; Seok, S.I.; Im, S.H.; Kim, S.O. Peptide-templating dye-sensitized solar cells. *Nanotechnology* **2010**, *21*, 185601. [[CrossRef](#)]
131. Niu, H.; Zhou, R.; Cheng, C.; Zhang, G.; Hu, Y.; Huang, B.; Zhang, S.; Shang, X.; Xia, M.; Xu, J. Magnetron sputtering in the creation of photonic nanostructures derived from Sasakia Charonda Formosana-butterfly wings for applied in dye-sensitized solar cells. *J. Power Sources* **2016**, *325*, 598–608. [[CrossRef](#)]
132. Zhang, G.; Wei, S.; Belcher, A.M. Biotemplated zinc sulfide nano fibers as anode materials for sodium-ion batteries. *ACS Appl. Nanomater.* **2018**, *1*, 5631–5639. [[CrossRef](#)]
133. Zilinskaite, S.; Rennie, A.J.R.; Boston, R.; Reeves-McLaren, N. Biotemplating: A sustainable synthetic methodology for Na-ion battery materials. *J. Mater. Chem. A* **2018**, *6*, 5346–5355. [[CrossRef](#)]
134. Xue, J.; Dou, G.; Ziade, E.; Goldfarb, J.L. Integrating sustainable biofuel and silver nanomaterial production for in situ upgrading of cellulosic biomass pyrolysis. *Energy Convers. Manag.* **2017**, *142*, 143–152. [[CrossRef](#)]
135. Ashman, C.H.; Gao, L.; Goldfarb, J.L. Silver nitrate in situ upgrades pyrolysis biofuels from brewer's spent grain via biotemplating. *J. Anal. Appl. Pyrolysis* **2020**, *146*, 104729. [[CrossRef](#)]
136. Chen, L.; Wang, X. Bio-templated Fabrication of Metal-Free Boron Carbonitride Tubes for Visible Light Photocatalysis. *Chem. Commun.* **2017**, *53*, 11988–11991. [[CrossRef](#)] [[PubMed](#)]
137. Hashemizadeh, I.; Golovko, V.B.; Choi, J.; Tsang, D.C.W.; Yip, A.C.K. Photocatalytic reduction of CO<sub>2</sub> to hydrocarbons using bio-templated porous TiO<sub>2</sub> architectures under UV and visible light. *Chem. Eng. J.* **2018**, *347*, 64–73. [[CrossRef](#)]
138. Martín-Gómez, J.; Hidalgo-Carrillo, J.; Estévez, R.C.; Urbano, F.J.; Marinas, A. Hydrogen photoproduction on TiO<sub>2</sub>-CuO artificial olive leaves. *Appl. Catal. A Gen.* **2021**, *620*, 118178. [[CrossRef](#)]
139. Lu, X.; Zhai, T.; Cui, H.; Shi, J.; Xie, S.; Huang, Y.; Liang, C.; Tong, Y. Redox cycles promoting photocatalytic hydrogen evolution of CeO<sub>2</sub> nanorods. *J. Mater. Chem.* **2011**, *21*, 5569–5572. [[CrossRef](#)]
140. Liu, C.; Sun, H.; Qian, J.; Chen, Z.; Lv, Y.; Chen, F.; Lu, X.; Wu, Z. Biotemplating synthesis and photocatalytic activities of N-doped CeO<sub>2</sub> microcapsule tailored by hemerocallis pollen. *Adv. Powder Technol.* **2017**, *28*, 2741–2746. [[CrossRef](#)]
141. Van Benthem, K.; Elsässer, C.; French, R.H. Bulk electronic structure of SrTiO<sub>3</sub>: Experiment and theory. *J. Appl. Phys.* **2001**, *90*, 6156–6164. [[CrossRef](#)]
142. Nuraje, N.; Lei, Y.; Belcher, A. Virus-templated visible spectrum active perovskite photocatalyst. *Catal. Commun.* **2014**, *44*, 68–72. [[CrossRef](#)]
143. Qin, L.; Si, G.; Li, X.; Kang, S.Z. Synergetic effect of Cu-Pt bimetallic cocatalyst on SrTiO<sub>3</sub> for efficient photocatalytic hydrogen production from water. *RSC Adv.* **2015**, *5*, 102593–102598. [[CrossRef](#)]
144. Azmy, H.A.M.; Razuki, N.A.; Aziz, A.W.; Satar, N.S.A.; Kaus, N.H.M. Visible light photocatalytic activity of BiFeO<sub>3</sub> nanoparticles for degradation of methylene blue. *J. Phys. Sci.* **2017**, *28*, 85–103. [[CrossRef](#)]
145. Yang, Z.; Kang, J.; Li, L.; Guo, L. A biotemplating route for the synthesis of hierarchical Fe<sub>2</sub>O<sub>3</sub> with highly dispersed carbon as electron-transfer channel. *Chempluschem* **2020**, *85*, 258–263. [[CrossRef](#)]
146. Gutbrod, K.; Greil, P.; Zollfrank, C. Carbon auto-doping improves photocatalytic properties of biotemplated ceramics. *Appl. Catal. B Environ.* **2011**, *103*, 240–245. [[CrossRef](#)]
147. Ivanova, A.; Fattakhova-Rohlfing, D.; Kayaalp, B.E.; Rathouský, J.; Bein, T. Tailoring the morphology of mesoporous titania thin films through biotemplating with nanocrystalline cellulose. *J. Am. Chem. Soc.* **2014**, *136*, 5930–5937. [[CrossRef](#)]
148. He, Z.; Que, W.; Chen, J.; He, Y.; Wang, G. Surface chemical analysis on the carbon-doped mesoporous TiO<sub>2</sub> photocatalysts after post-thermal treatment: XPS and FTIR characterization. *J. Phys. Chem. Solids* **2013**, *74*, 924–928. [[CrossRef](#)]
149. Mohamed, M.A.; Salleh, W.N.W.; Jaafar, J.; Mohd Hir, Z.A.; Rosmi, M.S.; Mutalib, M.A.; Ismail, A.F.; Tanemura, M. Regenerated cellulose membrane as bio-temple for in-situ growth of visible-light driven C-modified mesoporous titania. *Carbohydr. Polym.* **2016**, *146*, 166–173. [[CrossRef](#)]

150. Cai, Q.; Liu, C.; Yin, C.; Huang, W.; Cui, L.; Shi, H.; Fang, X.; Zhang, L.; Kang, S.; Wang, Y. Biotemplating synthesis of graphitic Carbon-coated TiO<sub>2</sub> and its application as efficient visible-light-driven photocatalyst for Cr<sup>6+</sup> remove. *ACS Sustain. Chem. Eng.* **2017**, *5*, 3938–3944. [[CrossRef](#)]
151. Magnabosco, G.; Papiano, I.; Aizenberg, M.; Aizenberg, J.; Falini, G. Beyond biotemplating: Multiscale porous inorganic materials with high catalytic efficiency. *Chem. Commun.* **2020**, *56*, 3389–3392. [[CrossRef](#)]
152. Xue, J.; Song, F.; Yin, X.W.; Zhang, Z.L.; Liu, Y.; Wang, X.L.; Wang, Y.Z. Cellulose nanocrystal-templated synthesis of mesoporous TiO<sub>2</sub> with dominantly exposed (001) facets for efficient catalysis. *ACS Sustain. Chem. Eng.* **2017**, *5*, 3721–3725. [[CrossRef](#)]
153. Shahini, P.; Ashkarran, A.A. TiO<sub>2</sub> nanofibers assembled on graphene-silver platform as a visible-light photo and bio-active nanostructure. *Ceram. Int.* **2017**, *43*, 8655–8663. [[CrossRef](#)]
154. Shafae, M.; Goharshadi, E.K.; Mashreghi, M.; Sadeghinia, M. TiO<sub>2</sub> nanoparticles and TiO<sub>2</sub>@graphene quantum dots nanocomposites as effective visible/solar light photocatalysts. *J. Photochem. Photobiol. A Chem.* **2018**, *357*, 90–102. [[CrossRef](#)]
155. Lu, X.; Li, X.; Chen, F.; Chen, Z.; Qian, J.; Zhang, Q. Biotemplating synthesis of N-doped two-dimensional CeO<sub>2</sub>-TiO<sub>2</sub> nanosheets with enhanced visible light photocatalytic desulfurization performance. *J. Alloys Compd.* **2020**, *815*, 152326. [[CrossRef](#)]
156. Serrà, A.; Artal, R.; García-Amorós, J.; Sepúlveda, B.; Gómez, E.; Nogués, J.; Philippe, L. Hybrid Ni@ZnO@ZnS-microalgae for circular economy: A smart route to the efficient integration of solar photocatalytic water decontamination and bioethanol production. *Adv. Sci.* **2020**, *7*, 1902447. [[CrossRef](#)]
157. Serrà, A.; Gómez, E.; Michler, J.; Philippe, L. Facile cost-effective fabrication of Cu@Cu<sub>2</sub>O@CuO-microalgae photocatalyst with enhanced visible light degradation of tetracycline. *Chem. Eng. J.* **2021**, *413*. [[CrossRef](#)]
158. Posa, V.R.; Annavaram, V.; Koduru, J.R.; Ammireddy, V.R.; Somala, A.R. Graphene-ZnO nanocomposite for highly efficient photocatalytic degradation of methyl orange dye under solar light irradiation. *Korean J. Chem. Eng.* **2016**, *33*, 456–464. [[CrossRef](#)]
159. Juárez, J.; Cambón, A.; Goy-López, S.; Topete, A.; Taboada, P.; Mosquera, V. Obtention of metallic nanowires by protein biotemplating and their catalytic application. *J. Phys. Chem. Lett.* **2010**, *1*, 2680–2687. [[CrossRef](#)]
160. Pushpavanam, K.; Santra, S.; Rege, K. Biotemplating Plasmonic nanoparticles using intact microfluidic vasculature of leaves. *Langmuir* **2014**, *30*, 14095–14103. [[CrossRef](#)]
161. Inbaraj, B.S.; Chen, B.; Liao, C.-W.; Chen, B.-H. Green synthesis, characterization and evaluation of catalytic and antibacterial activities of chitosan, glycol chitosan and poly ( $\gamma$ -glutamic acid) capped gold nanoparticles. *Int. J. Biol. Macromol.* **2020**, *161*, 1484–1495. [[CrossRef](#)] [[PubMed](#)]
162. Qin, L.; Liu, M.; Wu, Y.; Xu, Z.; Guo, X.; Zhang, G. Bioinspired hollow and hierarchically porous MO<sub>x</sub>(M =Ti, Si)/carbon microellipsoids supported with Fe<sub>2</sub>O<sub>3</sub> for heterogenous photochemical oxidation. *Appl. Catal. B Environ.* **2016**, *194*, 50–60. [[CrossRef](#)]
163. Liu, Y.; Wang, G.; Yang, W.; Yang, J.; Li, J. Biotemplated synthesis of hierarchically porous ZnAl-CLDH/FeWO<sub>4</sub> for effective removal of dyes from water. *Water. Air. Soil Pollut.* **2019**, *230*, 89. [[CrossRef](#)]
164. Jeevitha, G.; Abhinayaa, R.; Mangalaraj, D.; Ponpandian, N. Tungsten oxide-graphene oxide (WO<sub>3</sub>-GO) nanocomposite as an efficient photocatalyst, antibacterial and anticancer agent. *J. Phys. Chem. Solids* **2018**, *116*, 137–147. [[CrossRef](#)]
165. Qiu, Z.; Huang, H.; Du, J.; Tao, X.; Xia, Y.; Feng, T.; Gan, Y.; Zhang, W. Biotemplated synthesis of bark-structured TiC nanowires as Pt catalyst supports with enhanced electrocatalytic activity and durability for methanol oxidation. *J. Mater. Chem. A* **2014**, *2*, 8003–8008. [[CrossRef](#)]
166. Peng, M.; Qiao, Y.; Luo, M.; Wang, M.; Chu, S.; Zhao, Y.; Liu, P.; Liu, J.; Tan, Y. Bioinspired Fe<sub>3</sub>C@C as highly efficient electrocatalyst for nitrogen reduction reaction under ambient conditions. *ACS Appl. Mater. Interfaces* **2019**, *11*, 40062–40068. [[CrossRef](#)]
167. Records, W.C.; Yoon, Y.; Ohmura, J.F.; Chanut, N.; Belcher, A.M. Virus-templated Pt-Ni(OH)<sub>2</sub> nanonetworks for enhanced electrocatalytic reduction of water. *Nano Energy* **2019**, *58*, 167–174. [[CrossRef](#)]
168. Liu, Z.; Wang, X.; Mao, T.; Sima, J.; Gong, C.; Fan, G. Precise casting of biomorphic La<sub>0.9</sub>K<sub>0.1</sub>CoO<sub>3</sub> catalysts derived from pinewood for diesel soot combustion. *RSC Adv.* **2016**, *6*, 87856–87862. [[CrossRef](#)]
169. Bedford, N.M.; Ramezani-Dakhel, H.; Slocik, J.M.; Briggs, B.D.; Ren, Y.; Frenkel, A.I.; Petkov, V.; Heinz, H.; Naik, R.R.; Knecht, M.R. Elucidation of peptide-directed palladium surface structure for biologically tunable nanocatalysts. *ACS Nano* **2015**, *9*, 5082–5092. [[CrossRef](#)]
170. Linsha, V.; Aboo Shuhailath, K.; Mahesh, K.V.; Mohamed, A.A.P.; Ananthakumar, S. Biocatalytic conversion efficiency of steapsin lipase immobilized on hierarchically porous biomorphic aerogel supports. *ACS Sustain. Chem. Eng.* **2016**, *4*, 4692–4703. [[CrossRef](#)]
171. Akhavan, O.; Ghaderi, E. Photocatalytic reduction of graphene oxide nanosheets on TiO<sub>2</sub> thin film for photoinactivation of bacteria in solar light irradiation. *J. Phys. Chem. C* **2009**, *113*, 20214–20220. [[CrossRef](#)]
172. Akhavan, O.; Choobtashani, M.; Ghaderi, E. Protein degradation and RNA efflux of viruses photocatalyzed by graphene-tungsten oxide composite under visible light irradiation. *J. Phys. Chem. C* **2012**, *116*, 9653–9659. [[CrossRef](#)]
173. Akhavan, O.; Ghaderi, E.; Rahimi, K. Adverse effects of graphene incorporated in TiO<sub>2</sub> photocatalyst on minuscule animals under solar light irradiation. *J. Mater. Chem.* **2012**, *22*, 23260–23266. [[CrossRef](#)]
174. Akhavan, O. Lasting antibacterial activities of Ag-TiO<sub>2</sub>/Ag/a-TiO<sub>2</sub> nanocomposite thin film photocatalysts under solar light irradiation. *J. Colloid Interface Sci.* **2009**, *336*, 117–124. [[CrossRef](#)]
175. Galusha, J.W.; Richey, L.R.; Jorgensen, M.R.; Gardner, J.S.; Bartl, M.H. Study of natural photonic crystals in beetle scales and their conversion into inorganic structures via a sol-gel bio-templating route. *J. Mater. Chem.* **2010**, *20*, 1277–1284. [[CrossRef](#)]

176. Zampieri, A.; Mabande, G.T.P.; Selvam, T.; Schwieger, W.; Rudolph, A.; Hermann, R.; Sieber, H.; Greil, P. Biotemplating of *Luffa cylindrica* sponges to self-supporting hierarchical zeolite macrostructures for bio-inspired structured catalytic reactors. *Mater. Sci. Eng. C* **2006**, *26*, 130–135. [[CrossRef](#)]
177. Zhang, B.; Yang, S.; Zhang, Y.; Wang, Q.; Ren, T. Biotemplate-directed fabrication of size-controlled monodisperse magnetic silica microspheres. *Colloids Surfaces B Biointerfaces* **2015**, *131*, 129–135. [[CrossRef](#)]
178. Hussein, M.Z.; Azmin, W.H.W.N.; Mustafa, M.; Yahaya, A.H. *Bacillus cereus* as a biotemplating agent for the synthesis of zinc oxide with raspberry- and plate-like structures. *J. Inorg. Biochem.* **2009**, *103*, 1145–1150. [[CrossRef](#)]
179. Nomura, T.; Bando, M.; Konishi, Y. Facile fabrication of hollow titania microparticles using wet yeast cells as templates. *Colloids Surf. A Physicochem. Eng. Asp.* **2015**, *487*, 215–220. [[CrossRef](#)]
180. Korkmaz, N.; Arslan, T. Genetically engineered Fd viruses for site specific material binding. *Bionanoscience* **2019**, *9*, 862–872. [[CrossRef](#)]
181. Lu, Z.X.; Wood, L.F.; Ohman, D.E.; Collinson, M.M. Bio-inspired chemical reactors for growing aligned gold nanoparticle-like wires. *Chem. Commun.* **2009**, *28*, 4200–4202. [[CrossRef](#)]
182. Zhou, J.C.; Soto, C.M.; Chen, M.S.; Bruckman, M.A.; Moore, M.H.; Barry, E.; Ratna, B.R.; Pehrsson, P.E.; Spies, B.R.; Confer, T.S. Biotemplating rod-like viruses for the synthesis of copper nanorods and nanowires. *J. Nanobiotechnology* **2012**, *10*, 18. [[CrossRef](#)]
183. Kamata, K.; Piao, Z.; Suzuki, S.; Fujimori, T.; Tajiri, W.; Nagai, K.; Iyoda, T.; Yamada, A.; Hayakawa, T.; Ishiura, M.; et al. Spirulina-templated metal microcoils with controlled helical structures for THz electromagnetic responses. *Sci. Rep.* **2014**, *4*, 4919. [[CrossRef](#)] [[PubMed](#)]
184. Ölçeroğlu, E.; Hsieh, C.Y.; Rahman, M.M.; Lau, K.K.S.; McCarthy, M. Full-field dynamic characterization of superhydrophobic condensation on biotemplated nanostructured surfaces. *Langmuir* **2014**, *30*, 7556–7566. [[CrossRef](#)] [[PubMed](#)]
185. Zeni, T.L.; Rambo, C.R.; Magalhaes, W.L.E.; Hotza, D. Control of porosity and permeability of wood by fungi action for biotemplating of SiC. *J. Wood Chem. Technol.* **2013**, *33*, 33–43. [[CrossRef](#)]
186. Alloyear, D.; Stéphanidis, B.; Zhao, X.; Larquet, E.; Boisset, N.; Ricolleau, C. Biotemplated synthesis of metallic nanoclusters organized in tunable two-dimensional superlattices. *J. Phys. Chem. C* **2011**, *115*, 20926–20930. [[CrossRef](#)]
187. Bird, S.M.; Galloway, J.M.; Rawlings, A.E.; Bramble, J.P.; Staniland, S.S. Taking a hard line with biotemplating: Cobalt-doped magnetite magnetic nanoparticle arrays. *Nanoscale* **2015**, *7*, 7340–7351. [[CrossRef](#)] [[PubMed](#)]
188. Deplanche, K.; Woods, R.D.; Mikheenko, I.P.; Sockett, R.; Macaskie, L.E. Manufacture of Stable palladium and gold nanoparticles on native and genetically engineered flagella scaffolds. *Biotechnol. Bioeng.* **2008**, *101*, 873–880. [[CrossRef](#)]
189. Hüttel, R.; Ullrich, F.; Wolf, G.; Kirchner, A.; Mertig, M.; Pompe, W. Calorimetric methods for catalytic investigations of novel catalysts based on metallized S-layer preparations. *Thermochim. Acta* **2006**, *440*, 13–18. [[CrossRef](#)]
190. Kasotakis, E.; Mitraki, A. Silica biotemplating by self-assembling peptides via serine residues activated by the peptide amino terminal group. *Biopolymers* **2012**, *98*, 501–509. [[CrossRef](#)]
191. Jiang, Y.; Fu, J.; Pan, J.; An, Z.; Cai, J.; Zhang, D. Biopattern transfer using diatom frustules for fabrication of functional micro/nanostructures. *J. Micro Nanolithography MEMS MOEMS* **2015**, *14*, 014502. [[CrossRef](#)]
192. Juárez, J.; Cambón, A.; Topete, A.; Taboada, P.; Mosquera, V. One-dimensional magnetic nanowires obtained by protein fibril biotemplating. *Chem.-Eur. J.* **2011**, *17*, 7366–7373. [[CrossRef](#)]
193. Leroux, F.; Gysemans, M.; Bals, S.; Batenburg, K.J.; Snauwaert, J.; Verbiest, T.; Van Haesendonck, C.; Van Tendeloo, G. Three-dimensional characterization of helical silver nanochains mediated by protein assemblies. *Adv. Mater.* **2010**, *22*, 2193–2197. [[CrossRef](#)]
194. Liu, C.; Chung, S.H.; Jin, Q.; Sutton, A.; Yan, F.; Hoffmann, A.; Kay, B.K.; Bader, S.D.; Makowski, L.; Chen, L. Magnetic viruses via nano-capsid templates. *J. Magn. Magn. Mater.* **2006**, *302*, 47–51. [[CrossRef](#)]
195. Wnęk, M.; Górzny, M.L.; Ward, M.B.; Wälti, C.; Davies, A.G.; Brydson, R.; Evans, S.D.; Stockley, P.G. Fabrication and characterization of gold nano-wires templated on virus-like arrays of tobacco mosaic virus coat proteins. *Nanotechnology* **2013**, *24*, 025605. [[CrossRef](#)]
196. Huggins, K.N.L.; Schoen, A.P.; Arunagirinathan, M.A.; Heilshorn, S.C. Multi-site functionalization of protein scaffolds for bimetallic nanoparticle templating. *Adv. Funct. Mater.* **2014**, *24*, 7737–7744. [[CrossRef](#)]
197. Malisaukas, M.; Meskys, R.; Morozova-Roche, L.A. Ultrathin silver nanowires produced by amyloid biotemplating. *Biotechnol. Prog.* **2008**, *24*, 1166–1170. [[CrossRef](#)]
198. Schoen, A.P.; Schoen, D.T.; Huggins, K.N.L.; Arunagirinathan, M.A.; Heilshorn, S.C. Template engineering through epitope recognition: A modular, biomimetic strategy for inorganic nanomaterial synthesis. *J. Am. Chem. Soc.* **2011**, *133*, 18202–18207. [[CrossRef](#)]
199. Shindel, M.M.; Mumm, D.R.; Wang, S.W. Biotemplating of metallic nanoparticle arrays through site-specific electrostatic adsorption on streptavidin crystals. *Langmuir* **2010**, *26*, 11103–11112. [[CrossRef](#)]
200. Tang, J.; Badelt-Lichtblau, H.; Ebner, A.; Preiner, J.; Kraxberger, B.; Gruber, H.J.; Sleytr, U.B.; Ilk, N.; Hinterdorfer, P. Fabrication of highly ordered gold nanoparticle arrays templated by crystalline lattices of bacterial S-layer protein. *ChemPhysChem* **2008**, *9*, 2317–2320. [[CrossRef](#)]
201. Zhou, J.C.; Wang, X.; Xue, M.; Xu, Z.; Hamasaki, T.; Yang, Y.; Wang, K.; Dunn, B. Characterization of gold nanoparticle binding to microtubule filaments. *Mater. Sci. Eng. C* **2010**, *30*, 20–26. [[CrossRef](#)]

202. Sierra-Sastre, Y.; Choi, S.; Picraux, S.T.; Batt, C.A. Vertical growth of Ge nanowires from biotemplated Au nanoparticle catalysts. *J. Am. Chem. Soc.* **2008**, *130*, 10488–10489. [[CrossRef](#)] [[PubMed](#)]
203. Galloway, J.M.; Bird, S.M.; Talbot, J.E.; Shepley, P.M.; Bradley, R.C.; El-Zubir, O.; Allwood, D.A.; Leggett, G.J.; Miles, J.J.; Staniland, S.S.; et al. Nano- and micro-patterning biotemplated magnetic CoPt arrays. *Nanoscale* **2016**, *8*, 11738–11747. [[CrossRef](#)] [[PubMed](#)]
204. Han, T.H.; Oh, J.K.; Park, J.S.; Kwon, S.H.; Kim, S.W.; Kim, S.O. Highly entangled hollow TiO<sub>2</sub> nanoribbons templating diphenylalanine assembly. *J. Mater. Chem.* **2009**, *19*, 3512–3516. [[CrossRef](#)]
205. Nguyen, T.D.; Tang, D.; D’Acerno, F.; Michal, C.A.; MacLachlan, M.J. Biotemplated lightweight  $\gamma$ -Alumina aerogels. *Chem. Mater.* **2018**, *30*, 1602–1609. [[CrossRef](#)]
206. Sachse, A.; Cardoso, L.; Kostov, K.L.; Gérardin, C.; Belamie, E.; Alonso, B. Mesoporous alumina from colloidal biotemplating of Al clusters. *Chem.-Eur. J.* **2015**, *21*, 3206–3210. [[CrossRef](#)]
207. Sachse, A.; Hulea, V.; Kostov, K.L.; Belamie, E.; Alonso, B. Improved silica-titania catalysts by chitin biotemplating. *Catal. Sci. Technol.* **2015**, *5*, 415–427. [[CrossRef](#)]
208. Bai, H.; Xu, F.; Anjia, L.; Matsui, H. Low temperature synthesis of ZnO nanowires by using a genetically-modified collagen-like triple helix as a catalytic template. *Soft Matter* **2009**, *5*, 966–969. [[CrossRef](#)]
209. Kim, J.W.; Choi, S.H.; Lillehei, P.T.; Chu, S.H.; King, G.C.; Watt, G.W. Cobalt oxide hollow nanoparticles derived by bio-templating. *Chem. Commun.* **2005**, *28*, 4101–4103. [[CrossRef](#)]
210. Li, D.; Mathew, B.; Mao, C. Biotemplated synthesis of hollow double-layered core/shell titania/silica nanotubes under ambient conditions. *Small* **2012**, *8*, 3691–3697. [[CrossRef](#)]
211. Maheshkumar, J.; Sreedhar, B.; Nair, B.U.; Dhathathreyan, A. Supported lipid bilayers as templates to design manganese oxide nanoparticles. *J. Chem. Sci.* **2012**, *124*, 979–984. [[CrossRef](#)]
212. Ge, D.; Mu, J.; Huang, S.; Liang, P.; Gcilitshana, O.U.; Ji, S.; Linkov, V.; Shi, W. Electrochemical synthesis of polypyrrole nanowires in the presence of gelatin. *Synth. Met.* **2011**, *161*, 166–172. [[CrossRef](#)]
213. Chen, J.Y.; Yang, C.Y.; Chen, P.Y. Synthesis of hierarchically porous structured CaCO<sub>3</sub> and TiO<sub>2</sub> replicas by sol-gel method using lotus root as template. *Mater. Sci. Eng. C* **2016**, *67*, 85–97. [[CrossRef](#)]
214. Li, J.; Kwong, F.L.; Zhu, J.; Ng, D.H.L. Synthesis of biomorphic ZnO nanostructures by using the cetyltrimethylammonium bromide modified silk templates. *J. Am. Ceram. Soc.* **2010**, *93*, 3726–3731. [[CrossRef](#)]
215. Rambo, C.R.; Hotza, D. Microchanneled biomorphic AlN-coated Al<sub>2</sub>O<sub>3</sub> by pressureless infiltration-nitridation. *Ceram. Int.* **2014**, *40*, 12567–12571. [[CrossRef](#)]
216. Wang, C.; Li, J.; Paineau, E.; Laachachi, A.; Colbeau-Justin, C.; Remita, H.; Ghazzal, M.N. Sol-gel biotemplating route with cellulose nanocrystals to design a photocatalyst boosting the hydrogen generation. *J. Mater. Chem. A* **2020**, *8*, 10779–10786. [[CrossRef](#)]
217. Zhang, T.; Zhou, Y.; Wang, Y.; Bu, X.; Wang, H.; Zhang, M. Morphology-controlled fabrication of hierarchical LDH/C microspheres derived from rape pollen grain. *Appl. Clay Sci.* **2015**, *103*, 67–70. [[CrossRef](#)]
218. He, X.H.; Qi, L.H.; Wang, J.B.; Shen, M.Q.; Chang, W.; Fu, C.; Yang, M.G.; Su, X.L. Preparation of SnO<sub>2</sub>/C biomorphic materials by biotemplating from ramie fibres. *Bull. Mater. Sci.* **2011**, *34*, 1157–1162. [[CrossRef](#)]
219. Klaithong, S.; Van Opdenbosch, D.; Zollfrank, C.; Plank, J. Preparation of magnesium oxide and magnesium silicate replicas retaining the hierarchical structure of pine wood. *Zeitschrift fur Naturforsch. B* **2017**, *72*, 341–349. [[CrossRef](#)]
220. Ramimoghadam, D.; Hussein, M.Z.B.; Taufiq-Yap, Y.H. Synthesis and characterization of ZnO nanostructures using palm olein as biotemplate. *Chem. Cent. J.* **2013**, *7*, 71. [[CrossRef](#)]
221. Gruber, S.; Taylor, R.N.K.; Scheel, H.; Greil, P.; Zollfrank, C. Cellulose-biotemplated silica nanowires coated with a dense gold nanoparticle layer. *Mater. Chem. Phys.* **2011**, *129*, 19–22. [[CrossRef](#)]
222. Onyestyák, G. Pinewood char templated mordenite/carbon honeycomb composite. *New J. Chem.* **2006**, *30*, 1058–1064. [[CrossRef](#)]
223. Van Opdenbosch, D.; Fritz-Popovski, G.; Wagermaier, W.; Paris, O.; Zollfrank, C. Moisture-driven ceramic bilayer actuators from a biotemplating approach. *Adv. Mater.* **2016**, *28*, 5235–5240. [[CrossRef](#)] [[PubMed](#)]
224. Zampieri, A.; Kullmann, S.; Selvam, T.; Bauer, J.; Schwieger, W.; Sieber, H.; Fey, T.; Greil, P. Bioinspired Rattan-derived SiSiC/Zelite monoliths: Preparation and characterisation. *Microporous Mesoporous Mater.* **2006**, *90*, 162–174. [[CrossRef](#)]
225. Zampieri, A.; Sieber, H.; Selvam, T.; Mabande, G.T.P.; Schwieger, W.; Scheffler, F.; Scheffler, M.; Greil, P. Biomorphic cellular SiSiC/Zelite ceramic composites: From rattan palm to bioinspired structured monoliths for catalysis and sorption. *Adv. Mater.* **2005**, *17*, 344–349. [[CrossRef](#)]
226. Mroz, M.; Ali, M.; Howard, J.; Carlson, K.; Naleway, S.E. Biotemplating of a highly porous Cellulose–Silica composite from apium graveolens by a Low-Toxicity Sol–Gel technique. *JOM* **2021**, *73*, 1736–1744. [[CrossRef](#)]
227. Fritz-Popovski, G.; Morak, R.; Schöberl, T.; Van Opdenbosch, D.; Zollfrank, C.; Paris, O. Pore characteristics and mechanical properties of silica templated by wood. *Bioinspired Biomim. Nanobiomaterials* **2014**, *3*, 160–168. [[CrossRef](#)]
228. Onyestyák, G.; Valyon, J.; Papp, K. Novel biomorphous zeolite/carbon composite having honeycomb structure. *Mater. Sci. Eng. A* **2005**, *412*, 48–52. [[CrossRef](#)]
229. Qian, J.; Wang, J.; Hou, G.; Qiao, G.; Jin, Z. Preparation and characterization of biomorphic SiC hollow fibers from wood by chemical vapor infiltration. *Scr. Mater.* **2005**, *53*, 1363–1368. [[CrossRef](#)]
230. Cao, J.; Rambo, C.R.; Sieber, H. Preparation of porous Al<sub>2</sub>O<sub>3</sub> ceramics by biotemplating of wood. *J. Porous Mater.* **2004**, *11*, 163–172. [[CrossRef](#)]



231. Rambo, C.R.; Cao, J.; Sieber, H. Preparation and properties of highly porous, biomorphic YSZ ceramics. *Mater. Chem. Phys.* **2004**, *87*, 345–352. [[CrossRef](#)]
232. Sieber, H.; Rambo, C.; Cao, J.; Vogli, E.; Greil, P. Manufacturing of porous oxide ceramics by replication of plant morphologies. *Key Eng. Mater.* **2001**, 206–213, 2009–2012. [[CrossRef](#)]
233. Vogli, E.; Sieber, H.; Greil, P. Biomorphic SiC-Ceramic prepared by Si-Gas phase infiltration of wood. *J. Eur. Ceram. Soc.* **2002**, *22*, 2663–2668. [[CrossRef](#)]
234. Zollfrank, C.; Kladny, R.; Sieber, H.; Greil, P. Biomorphous SiOC/C-ceramic composites from chemically modified wood templates. *J. Eur. Ceram. Soc.* **2004**, *24*, 479–487. [[CrossRef](#)]
235. Rambo, C.R.; Bernardes, J.C.; Sieber, H.; Müller, D. Synthesis of biomorphic ZrC/C ceramics from rattan through zirconium oxychloride infiltration and carbothermal reduction. *J. Porous Mater.* **2021**, *28*, 157–163. [[CrossRef](#)]
236. Gómez-Martín, A.; Orihuela, M.P.; Ramírez-Rico, J.; Chacartegui, R.; Martínez-Fernández, J. Thermal conductivity of porous biomorphic SiC derived from wood precursors. *Ceram. Int.* **2016**, *42*, 16220–16229. [[CrossRef](#)]
237. Rambo, C.R.; Cao, J.; Rusina, O.; Sieber, H. Manufacturing of biomorphic (Si, Ti, Zr)-carbide ceramics by sol-gel processing. *Carbon* **2005**, *43*, 1174–1183. [[CrossRef](#)]
238. Sieber, H.; Hoffmann, C.; Kaindl, A.; Greil, P. Biomorphic cellular ceramics. *Adv. Eng. Mater.* **2000**, *2*, 105–109. [[CrossRef](#)]
239. Zhurinsh, A.; Locs, J.; Berzina-Cimdina, J. Investigation of the feasibility of pyrolytic obtaining of porous biomorphic SiC ceramics. *J. Anal. Appl. Pyrolysis* **2009**, *85*, 544–548. [[CrossRef](#)]
240. Zollfrank, C.; Sieber, H. Microstructure and phase morphology of wood derived biomorphous SiSiC-ceramics. *J. Eur. Ceram. Soc.* **2004**, *24*, 495–506. [[CrossRef](#)]
241. Du, J.; Yang, Y.; Fan, Z.; Xia, Y.; Cheng, X.; Gan, Y.; Hang, H.; Dong, L.; Li, X.; Zhang, W.; et al. Biotemplating fabrication, mechanical and electrical characterizations of NbC nanowire arrays from the bamboo substrate. *J. Alloys Compd.* **2013**, *560*, 142–146. [[CrossRef](#)]
242. Kamata, K.; Suzuki, S.; Ohtsuka, M.; Nakagawa, M.; Iyoda, T.; Yamada, A. Fabrication of left-handed metal microcoil from spiral vessel of vascular plant. *Adv. Mater.* **2011**, *23*, 5509–5513. [[CrossRef](#)]
243. Schnepf, Z.; Yang, W.; Antonietti, M.; Giordano, C. Biotemplating of metal carbide microstructures: The magnetic leaf. *Angew. Chem.-Int. Ed.* **2010**, *49*, 6564–6566. [[CrossRef](#)]
244. Zheng, C.; Li, Z.; Xu, T.; Chen, L.; Fang, F.; Wang, D.; Dai, P.; Wang, Q.; Wu, X.; Yan, X. Spirulina-templated porous hollow carbon@magnetite core-shell microswimmers. *Appl. Mater. Today* **2021**, *22*, 100962. [[CrossRef](#)]
245. Elfving, A.; Ponseca, C.S.; Ouyang, L.; Urbanowicz, A.; Krotkus, A.; Tu, D.; Forchheimer, R.; Inganäs, O. Conducting helical structures from celery decorated with a metallic conjugated polymer give resonances in the terahertz range. *Adv. Funct. Mater.* **2018**, *28*, 1706595. [[CrossRef](#)]
246. Kostova, M.H.; Batentschuk, M.; Goetz-Neunhoffer, F.; Gruber, S.; Winnacker, A.; Greil, P.; Zollfrank, C. Biotemplating of BaFBr:Eu<sup>2+</sup> for X-ray storage phosphor applications. *Mater. Chem. Phys.* **2010**, *123*, 166–171. [[CrossRef](#)]
247. Krzesińska, M.; Pilawa, B.; Pusz, S.; Ng, J. Physical characteristics of carbon materials derived from pyrolysed vascular plants. *Biomass Bioenergy* **2006**, *30*, 166–176. [[CrossRef](#)]
248. Raja, M.W.; Islam, Q.A.; Basu, R.N. Oxygen separation membrane derived from aquatic weed: A novel bio-inspired approach to synthesize BaBi<sub>0.2</sub>Co<sub>0.35</sub>Fe<sub>0.45</sub>O<sub>3-δ</sub> perovskite from water hyacinth (*Eichhornia crassipes*). *J. Memb. Sci.* **2017**, *522*, 168–174. [[CrossRef](#)]
249. Cohen-Hadar, N.; Wine, Y.; Lagziel-Simis, S.; Moscovich-Dagan, H.; Dror, Y.; Frolow, F.; Freeman, A. Protein Crystal-mediated biotemplating. *J. Porous Media* **2009**, *12*, 213–220. [[CrossRef](#)]
250. Prekajski, M.; Babić, B.; Bučevac, D.; Pantić, J.; Gulicovski, J.; Miljković, M.; Matović, B. Synthesis and characterization of biomorphic CeO<sub>2</sub> obtained by using egg shell membrane as template. *Process. Appl. Ceram.* **2014**, *8*, 81–85. [[CrossRef](#)]
251. Sabu, U.; Tripathi, N.; Logesh, G.; Rashad, M.; Joy, A.; Balasubramanian, M. Development of biomorphic C-ZnO with in situ formation of ZnS using eggshell membrane as bio-template. *Ceram. Int.* **2020**, *46*, 22869–22875. [[CrossRef](#)]
252. Sabu, U.; Kumar, C.N.S.; Logesh, G.; Rashad, M.; Melinte, G.; Joy, A.; Kübel, C.; Balasubramanian, M. On the formation of α-alumina single crystal platelets through eggshell membrane bio-templating. *Scr. Mater.* **2021**, *195*, 113716. [[CrossRef](#)]
253. Dong, Q.; Su, H.; Zhang, D.; Liu, Z.; Lai, Y. Synthesis of hierarchical mesoporous titania with interwoven networks by eggshell membrane directed sol-gel technique. *Microporous Mesoporous Mater.* **2007**, *98*, 344–351. [[CrossRef](#)]
254. Dietrich, D.; Viney, M.; Lampke, T. Petrifications and wood-templated ceramics: Comparisons between natural and artificial silicification. *IAWA J.* **2015**, *36*, 167–185. [[CrossRef](#)]
255. Matovic, B.; Nikolic, D.; Labus, N.; Ilic, S.; Maksimovic, V.; Lukovic, J.; Bucevac, D. Preparation and properties of porous, biomorphic, ceria ceramics for immobilization of Sr isotopes. *Ceram. Int.* **2013**, *39*, 9645–9649. [[CrossRef](#)]
256. Hoppe, R.H.W.; Petrova, S.I. Optimal shape design in biomimetics based on homogenization and adaptivity. *Math. Comput. Simul.* **2004**, *65*, 257–272. [[CrossRef](#)]
257. Cohen-Hadar, N.; Wine, Y.; Nachliel, E.; Huppert, D.; Gutman, M.; Frolow, F.; Freeman, A. Monitoring The stability of crosslinked protein crystals biotemplates: A feasibility study. *J. Anat.* **2006**, *94*, 1005–1011. [[CrossRef](#)]
258. Rahman, M.M.; Ölçeroglu, E.; McCarthy, M. Role of wickability on the critical heat flux of structured superhydrophilic surfaces. *Langmuir* **2014**, *30*, 11225–11234. [[CrossRef](#)]

- 
259. Mathew, M.; Wisner, B.; Ridwan, S.; McCarthy, M.; Bartoli, I.; Kotsos, A. A Bio-inspired frequency-based approach for tailorable and scalable speckle pattern generation. *Exp. Mech.* **2020**, *60*, 1103–1117. [[CrossRef](#)]
  260. Cai, J.; Wang, Z.; Wang, M.; Zhang, D. Au nanoparticle-grafted hierarchical pillars array replicated from diatom as reliable SERS substrates. *Appl. Surf. Sci.* **2021**, *541*, 148374. [[CrossRef](#)]
  261. Engbert, A.; Plank, J. Templating effect of alginate and related biopolymers as hydration accelerators for calcium alumina cement—A mechanistic study. *Mater. Des.* **2020**, *195*, 109054. [[CrossRef](#)]
  262. Northcutt, R.G.; Sundaresan, V.B. Phospholipid vesicles as soft templates for electropolymerization of nanostructured polypyrrole membranes with long range order. *J. Mater. Chem. A* **2014**, *2*, 11784–11791. [[CrossRef](#)]
  263. Nergiz, S.Z.; Slocik, J.M.; Naik, R.R.; Singamaneni, S. Surface defect sites facilitate fibrillation: An insight into adsorption of gold-binding peptides on Au(111). *Phys. Chem. Chem. Phys.* **2013**, *15*, 11629–11633. [[CrossRef](#)] [[PubMed](#)]